Received: 9 August 2018 | Revised: 24 February 2019 | Accepted: 28 February 2019

DOI: 10.1002/gj.3512

RESEARCH ARTICLE

WILEY

Ultramafic–mafic and granitoids supra-subduction magmatism in the southern Ashanti volcanic belt, Ghana: Evidence from geochemistry and Nd isotopes

Samuel B. Dampare[1,2] | Tsugio Shibata[3] | Daniel K. Asiedu[4] | Osamu Okano[3] | Shiloh K.D. Osae[1,2] | David Atta-Peters[4] | Patrick A. Sakyi[4]

[1] School of Nuclear and Allied Sciences, University of Ghana-Atomic, Legon-Accra, Ghana

[2] National Nuclear Research Institute, Ghana Atomic Energy Commission, Legon-Accra, Ghana

[3] Department of Earth Sciences, Okayama University, Okayama, Japan

[4] Department of Earth Science, University of Ghana, Legon-Accra, Ghana

Correspondence
Samuel B. Dampare, School of Nuclear and Allied Sciences, University of Ghana-Atomic, P.O. Box LG 80, Legon-Accra, Ghana.
Email: sbdampare@ug.edu.gh

Funding information
Japanese Government (Monbukagakusho: MEXT) and Okayama University; National Nuclear Research Institute (NNRI) of the Ghana Atomic Energy Commission (GAEC)

Handling Editor: Y. Liu

Geochemical and Nd isotope data are presented for Palaeoproterozoic ultramafic to mafic rocks and granitoids which are associated with volcanic rocks in the southern part of the Ashanti greenstone belts of Ghana. The Prince's Town granitoids display subduction-zone geochemical features, with some showing signatures similar to high-SiO_2 adakites (HSA). Their initial ε_{Nd} (2.1 Ga) values range from −1.01 to +2.92, and they have T_{DM2} of 2.17–2.51 Ga. The gabbros show slightly LREE-depleted and -enriched patterns, Th–U troughs, negative Nb, Zr–Hf and Ti anomalies, spikes in Sr and Pb, have ε_{Nd} (2.1 Ga) values ranging from −1.23 to +5.23, and T_{DM2} values from 2.08 to 2.57 Ga. The Ahama ultramafic body is characterized by two groups of pyroxenites. Both groups show LREE enrichment patterns, display Th–U and Nb–Ta troughs, minor or pronounced negative Zr–Hf and Ti anomalies. However, the Group I pyroxenites exhibit minor Ce anomalies and lower total REE contents (28.1–32.8 ppm) whereas Group II pyroxenites show significant negative Ce anomalies and relatively higher total REE contents of 57.1–124 ppm. The pyroxenites show negative initial ε_{Nd} (2.1 Ga) values (−0.58 to −5.68) and have T_{DM2} values of 2.52 to 2.75 Ga. The pyroxenitic and gabbroic rocks were most likely originated from a subduction-related lithospheric mantle. The Aketakyi ultramafic–mafic complex is made up of mainly cumulate dunite, harzburgite, pyroxenites, and gabbro. The rocks display LREE-depleted to flat patterns with low total REE contents (1.71 to 22.3 ppm) and demonstrate a supra-subduction affinity. They show high positive initial ε_{Nd} (2.1 Ga) values (+3.69 to +4.93), and T_{DM2} values of 1.99 to 2.04 Ga, which suggest that they were derived from depleted mantle magmas and were juvenile at their time of formation. The Nd isotopic data provides evidence for a possible contamination of the juvenile Birimian crust of the southern Ashanti belt by some amount of a pre-Birimian (or Archaean?) crustal material. The trace element and isotopic signatures as well as the field relations of the studied granitoids and mafic–ultramafic rocks show they were derived through supra-subduction-related magmatism during the Palaeoproterozoic.

KEYWORDS

Birimian, geochemistry, mafic–ultramafic rocks, Nd isotopes, Palaeoproterozoic

1 | INTRODUCTION

Palaeoproterozoic (Birimian) rocks form a significant part of the West African Craton (WAC; Figure 1). The Palaeoproterozoic and Archaean terranes of the WAC have been recognized as a major zone of crustal growth (e.g., Abouchami, Boher, Michard, & Albarede, 1990; Boher, Abouchami, Michard, Albarède, & Arndt, 1992; Taylor, Moorbath, Leube, & Hirdes, 1992). It has been shown from a large-scale isotopic studies that the main Palaeoproterozoic crustal growth event (or Eburnean orogeny) in the WAC represents major juvenile crust-forming process with involvement of only a negligible Archaean crustal components (e.g., Abouchami et al., 1990; Boher et al., 1992; Liégeois, Claessens, Camara, & Klerkx, 1991; Pawlig et al., 2006; Taylor et al., 1992). The Palaeoproterozoic terranes of the WAC greatly resemble the Archaean greenstone terranes, particularly in their structural style and composition, and like the Archaean, are surrounded with controversies regarding the tectonic processes that formed them. In terms of the tectonic setting in which the rocks were formed, interpretations vary between generation of the Birimian juvenile crust in arc environments (e.g., Asiedu et al., 2004; Dampare et al., 2008; Mortimer, 1992; Pohl & Carlson, 1993; Sylvester & Attoh, 1992) or from plume-related magmatism (e.g., Abouchami et al., 1990). Most of these models were based on isotopic and geochemical compositions of volcanic rocks from these greenstone belts, with some contributions from the sedimentary units and the associated granitoid intrusions, whereas the associated mafic–ultramafic intrusives have received little attention. Although voluminously minor, the mafic–ultramafic rocks may provide useful information to enable us to understand the geodynamic evolution of the Palaeoproterozoic greenstone belts. The mafic–ultramafic rocks and the granitoids are believed to provide evidence for juvenile crust-forming events near the Archaean–Proterozoic boundary (Attoh & Ekwueme, 1997; Hirdes & Davis, 2002; Taylor et al., 1992).

Several ultramafic–mafic intrusives are associated with the volcanic rocks and granitoids in the Palaeoproterozoic southern Ashanti greenstone belt of Ghana. These include the Aketakyi ultramafic complex (the largest ultramafic–mafic body in Ghana), the Ahama ultramafic body, and the Axim, Kegyina, and Aketakyi mafic bodies. This study has focused on the intrusive rocks in the Axim–Aketakyi area of the southern Ashanti volcanic belt. Consequently, the Prince's Town pluton is considered here together with the mafic–ultramafic rocks to enhance our understanding of the geodynamic setting of the greenstone belt. Petrographic and geochemical studies of some of the representative intrusions are available in Loh and Hirdes (1999) and

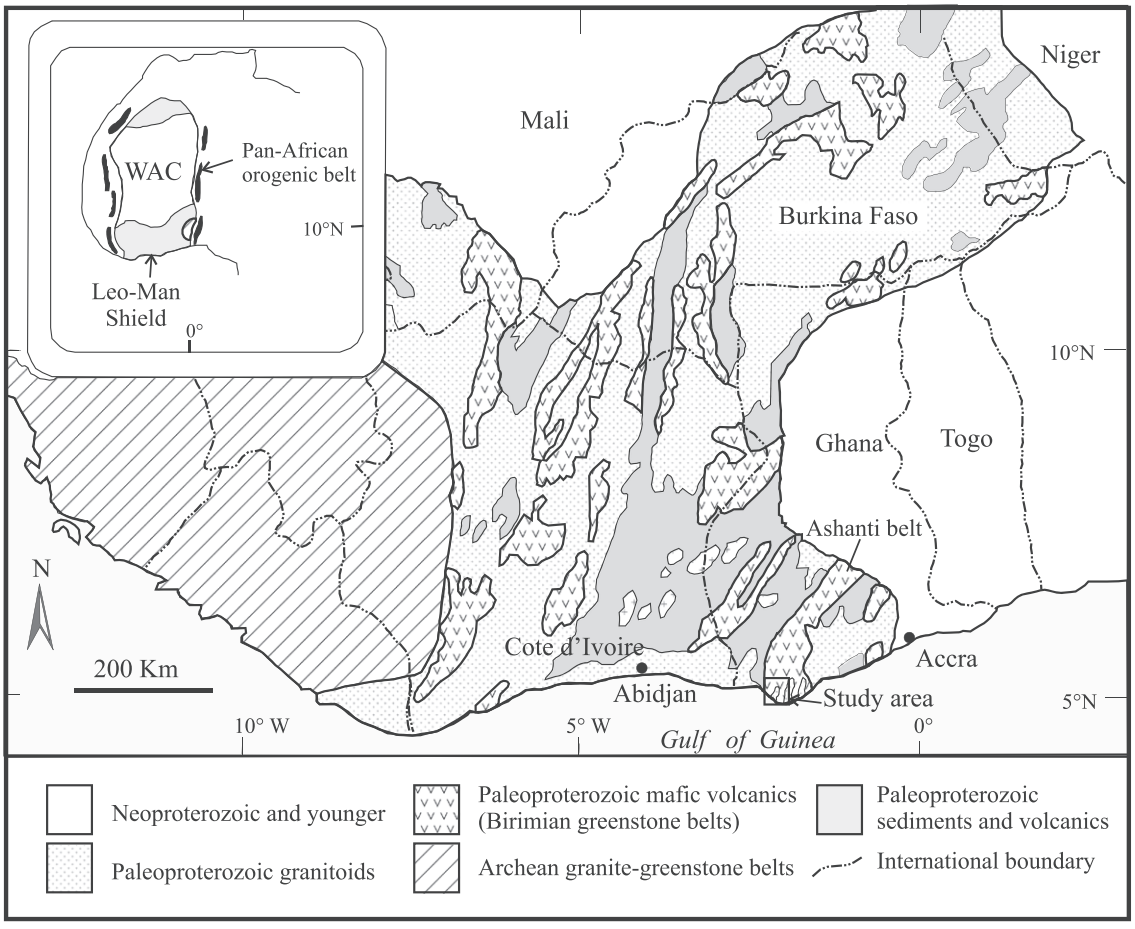

FIGURE 1 Geologic sketch of the Leo-Man Shield of the West Africa Craton (WAC; inset) showing the Palaeoproterozoic (Birimian) greenstone belts and the location of the study area (adopted after Attoh, Evans, & Bickford, 2006)

Attoh et al. (2006) and provide important background information for this study. The objectives of this paper are (a) to present chemical data of Palaeoproterozoic plutonic rocks exposed in the southern Ashanti greenstone terrane in south-western Ghana and (b) to discuss the petrogenesis of the plutonic rocks and the tectonic setting during their emplacement.

2 | GEOLOGICAL SETTING

Palaeoproterozoic rocks of the Birimian terrane of the Leo-Man Shield (Figure 1) form a significant portion of the WAC (Bessoles, 1977) to the east and north of the Archaean Liberian cratonic nucleus. The Palaeoproterozoic terrane, characterized by narrow sedimentary basins and linear, arcuate volcanic belts, is intruded by several generations of granitoids (Doumbia et al., 1998; Hirdes, Davis, Lüdtke, & Konan, 1996; Leube, Hirdes, Mauer, & Kesse, 1990) and corresponds to a period of accretion during the 2.1–2.0 Ga Eburnean orogeny (e.g., Abouchami et al., 1990). The Eburnean tectono-thermal event was not only accompanied by the deformation and the emplacement of syn- to post-orogenic tonalite–trondhjemite–granodiorite (TTG) and granite plutons along fractures (e.g., Feybesse et al., 2006; Leube et al., 1990; Vidal & Alric, 1994) but also resulted in widespread metamorphism mostly under greenschist-facies conditions (e.g., Oberthür, Vetter, Davis, & Amanor, 1998; Béziat et al., 2000). Also, evidence of medium amphibolite–facies metamorphism may be observed in the vicinity of granitoid plutons (e.g., Debat et al., 2003; Eisenlohr & Hirdes, 1992; Junner, 1940). Recently, John, Klemd, Hirdes, and Loh (1999), on the basis of mineral chemistry, have suggested that the entire Ashanti belt of south-eastern Ghana underwent epidote–amphibolite–facies metamorphism (T = 500–650°C and P = 5–6 kbar) before experiencing retrograde metamorphism under the greenschist-facies conditions.

2.1 | Lithostratigraphy

The lithostratigraphic succession of these Palaeoproterozoic rocks (i.e., the volcano-sedimentary and bimodal volcanics) has over the years been contentious with respect to whether the sedimentary unit lies below (e.g., Feybesse & Milési, 1994; Junner, 1940; Milési, Ledru, Feybesse, Dommanget, & Marcoux, 1992) or above (e.g., Asiedu et al., 2004; Hirdes et al., 1996; Tagini, 1971) the volcanic unit. It is now widely accepted that the two units formed quasi-contemporaneously, as lateral facies equivalents (e.g., Leube et al., 1990). According to Béziat et al. (2008), the lithostratigraphic succession of the Birimian crust sensu lato could be established from bottom to top as (a) a thick sequence of mafic rocks, including basalt, locally pillowed, as well as dolerite and gabbro, all of tholeiitic composition, locally interlayered with immature detrital sediments and limestone; (b) a detrital sedimentary pile (volcanics, turbidite, mudstone and carbonate) including interbedded calc-alkaline volcanics; and (c) a coarse clastic sedimentary sequence belonging to the Tarkwaian Group.

2.1.1 | Sediments and volcanics

The Palaeoproterozoic supracrustal rocks of Ghana are subdivided into the Birimian and Tarkwaian. The Birimian rocks comprise a series of subparallel, roughly equal-spaced north-east trending volcanic belts of volcanic rocks separated by an assemblage of volcano-sedimentary rocks. Traditionally, the Birimian rocks were classified into a two-fold lithostratigraphic and chronological system, consisting of an older metasedimentary sequence (referred to as Lower Birimian) and a younger volcanic sequence of predominantly tholeiitic basalt volcanic and pyroclastic rocks (referred to as Upper Birimian; e.g., Junner, 1940). Leube et al. (1990) have indicated that the volcanic and sedimentary rock sequences formed contemporaneously as lateral facies equivalents. The Birimian rocks are overlain by the detrital Tarkwaian sedimentary rocks in almost all the prominent volcanic belts, and both formations were subjected to similar deformation events, which involved compression along a southeast - northwest-trending axis, resulting in folding and thrusting with subsequent flattening and localized oblique-slip shearing (e.g., Allibone et al., 2002; Blenkinsop, Schmidt-Mumm, Kumi, & Sangmor, 1994; Eisenlohr, 1989; Eisenlohr & Hirdes, 1992). The Tarkwaian rocks are made up of conglomerates, sandstones, and subordinate shale, with much of the clastic material in the sediments derived from the adjacent Birimian units (Tunks, Selley, Rogers, & Brabham, 2004).

Radiometric dating on the Birimian of Ghana indicates that volcanic belts were deposited between 2,240 and 2,186 Ma whereas the sediments were deposited 100–60 Ma later into basins (Davis, Hirdes, Schaltegger, & Nunoo, 1994; Leube et al., 1990; Oberthür et al., 1998; Pigois, Groves, Fletcher, McNaughton, & Snee, 2003). Recently, on the basis of SHRIMP U–Pb analyses of detrital zircons, Pigois et al. (2003) have constrained the maximum age of sedimentation of the Tarkwaian to 2,133 ± 4 Ma. The Birimian and Tarkwaian rocks host the major gold deposits in Ghana, with most of the gold deposits concentrated along the western flank of the Ashanti belt. The major epigenetic lode-gold event occurred late in the Eburnean orogeny, after the peak of metamorphism was reached (John et al., 1999; Oberthür et al., 1998; Pigois et al., 2003; Yao et al., 2001). Using hydrothermal rutile, Oberthür et al. (1998) have obtained the age of hydrothermal alteration to be 2,092 ± 3 and 2,086 ± 4 Ma. Recently, Pigois et al. (2003) have determined the most robust age of 2,063 ± 9 Ma for gold mineralization in Ghana from SHRIMP II U–Pb analyses of hydrothermal xenotime.

2.1.2 | Granites

The Palaeoproterozoic granitoids have been classified into two main groups according to the presence or absence of amphibole (Lompo, 2009 and references therein): (a) the amphibole-bearing granitoids (PAG) and (b) the biotite ± muscovite-bearing granitoids without amphibole (PBG). The PAG granitoids are syntectonic intrusives in the greenstone terranes and are older than the PBG granitoids, which intrude the greenstone belts or the PAG granitoids (Lompo, 2009). On the basis of $^{207}Pb/^{206}Pb$ and U–Pb zircon geochronological data, two

main coeval plutonism and volcanism have been recognized and considered to mark two successive major episodes (i.e., Birimian sensu stricto [2,185–2,150 Ma] and Bandamian [2,115–2,100 Ma]) of Palaeoproterozoic crust formation in the West African Craton (Doumbia et al., 1998; Hirdes et al., 1996; Hirdes & Davis, 2002). However, the occurrence of some pre-Birimian ages in detrital zircons (2,245–2,266 Ma) from the Tarkwaian sediments (Davis et al., 1994; Loh & Hirdes, 1999), in two zircon grains (2,208 and 2,220 Ma) from the Tafolo tonalite (Doumbia et al., 1998), in zircon cores from the Issia granite (2,212–2,305 Ma) in south-western Cote d'Ivoire (Kouamelan, 1996; Kouamelan, Delor, & Peucat, 1997), and in zircon cores from the Dabakala tonalite (2,312 ± 17 Ma; Gasquet, Barbey, Adou, & Paquette, 2003) could probably suggest a pre-Birimian crustal growth episode.

The Birimian terrane of Ghana is intruded by two main suites of granitoids, namely, the Dixcove- (or belt-type) and Cape Coast-type (or basin-type) granitoids. The metaluminous, relatively Na-rich, Dixcove-type granitoids, which are dominantly hornblende- to biotite-bearing granodiorite to diorite, monzonite and syenite, intrude the Birimian volcanic belts and they may be coeval with the volcanic rocks (Eisenlohr & Hirdes, 1992). On the other hand, the Cape Coast-type granitoids, which are predominantly peraluminous, two-mica granodiorites, with lesser hornblende- and biotite-bearing granodiorites, are emplaced within the Birimian sedimentary basins. The Dixcove granitoids have been dated at 2,172 ± 1.4 Ma in the Ashanti Belt (Hirdes, Davis, & Eisenlohr, 1992) and the Cape Coast type between 2,104 ± 2 and 2,123 ± 3 Ma in the Kumasi Basin (Oberthür et al., 1998). Other types of granitoids include the localized, biotite and hornblende Winneba granitoids, and the K-rich Bongo granitoids which cut the Tarkwaian rocks in the volcanic belts. The Cape Coast-, Kumasi-, Dixcove-, and Bongo-type granitoids have strong mantle affinities whereas the Winneba type has an Archaean sialic precursor (Sm–Nd model age of ~2.6 Ga; Taylor et al., 1992). The Winneba-type granitoids are believed to be the only rock suite in Ghana which show evidence for a significant magmatic contribution from an Archaean continental crust in their genesis.

2.1.3 | Mafic and ultramafic rocks

The Birimian greenstone terrane is often characterized by metavolcanic and metasedimentary rocks, which have been intruded by granitoids and other mafic intrusive rocks. According to Béziat et al. (2000), the Birimian mafic suite comprises both volcanic rocks and plutonic complexes (ultrabasites and gabbros). Some of these plutonic complexes appear to outcrop over wide areas; these include the ultrabasic bodies at the eastern border of the Mako series, Eastern Senegal and those from the Ashanti belt of Ghana.

As intimated earlier, discussions on the processes of growth of the Proterozoic continental crust have mainly been driven by isotopic and geochemical compositions of volcanic rocks from these greenstone belts, with some contributions from the sedimentary units and the associated granitoid intrusions. In spite of the fact that the mafic–ultramafic rocks are voluminously minor, they could still provide useful information to enable us to understand the geodynamic evolution of the Palaeoproterozoic greenstone belts. For example, Béziat et al. (2000) have interpreted the Loraboué Birimian ultramafic–mafic assemblage, outcropping in the Boromo greenstone belt of Burkina Faso as the remains of a magma chamber that crystallized at the base of an island arc. Also, Attoh et al. (2006) have suggested that the rodingite-bearing ultramafic complex and associated pillowed basalts located in the Palaeoproterozoic (Birimian) Dixcove greenstone belt in south-western Ghana may represent fragments of a Palaeoproterozoic oceanic lithosphere.

In the study area, ultramafic to mafic complexes as well as isolated mafic bodies are associated with this greenstone–granitoid belt. The mafic and ultramafic rocks form a minor part of the entire intrusive bodies in the belt. The mafic rocks include the Axim gabbro, Kegyina gabbro and gabbroic rocks from the Aketakyi area. These mafic bodies appear to have been emplaced at different times (Loh & Hirdes, 1999).

Ultramafic rocks occur as two discrete bodies, namely, the Aketakyi ultramafic complex and the Ahama ultramafic body. Both bodies were emplaced in volcanic rocks and are separated by the Prince's Town granitoid body with the Ahama ultramafic body located to the west and the Aketakyi ultramafic complex to the east of the granitoid body.

2.2 | Tectonic setting

2.2.1 | Models

The context of crustal accretion and overall tectonic regime of the Palaeoproterozoic (Birimian) rocks has been a subject of contrasted interpretations. In terms of the tectonic setting in which the rocks were formed, interpretations vary between generation of the Birimian juvenile crust in arc environments (e.g., Asiedu et al., 2004; Dampare, Shibata, Asiedu, & Osae, 2005; Mortimer, 1992; Pohl & Carlson, 1993; Sylvester & Attoh, 1992) and from plume-related magmatism (e.g., Abouchami et al., 1990; Lompo, 2009). Two main models have been proposed to account for the tectonic processes involved in the formation of the rocks: accretionary orogeny versus transcurrent tectonics models. In the first model, the Eburnean event is seen as the accretionary orogeny that resulted from the collisions of island arcs and oceanic plateaus with an Archaean craton. In this case, the Eburnean is considered to be part of a much larger accretionary event that involved fragments of Precambrian crust now preserved over large parts of Africa and South America (Abouchami et al., 1990; Boher et al., 1992; Davis et al., 1994; Feybesse & Milési, 1994; Hirdes et al., 1996; Hirdes & Davis, 2002; Ledru, Johan, Milési, & Tegyey, 1994). The proponents of the second model intimate that the Palaeoproterozoic terranes are largely the product of transcurrent tectonics either in an oceanic domain that differentiated to produce continental crust or in association with Archaean basement but lacked any clear evidence of collisional processes (e.g., Bassot, 1987; Doumbia et al., 1998; Kouamelan, 1996). Apart from these two main models, there are some workers who favour the involvement of subduction processes in the generation of the Palaeoproterozoic terranes but

prefer small-scale extensional and accretionary processes to a large-scale collision (Ama-Salah, 1996; Vidal & Alric, 1994).

The tectonic setting in which the Palaeoproterozoic rocks of Ghana formed is contentious. One of the popular views is the tectonic model proposed by Leube et al. (1990), where an evolution of the tectonic setting of the Birimian/Eburnean in Ghana from an intracratonic-rift to oceanic-spreading and finally to an accretion–collision-related setting is envisaged. The Birimian volcanic belts originated as chains of volcanic islands developed during intracontinental rifting. The pyroclastic rocks which erupted from the volcanoes and epiclastic erosion products of the volcanic belts were deposited synchronously in adjacent subsiding basins to form the Birimian sediments. The geochronological and isotopic data suggest that the Birimian of Ghana represents a major Early Proterozoic magmatic crust-forming event around 2.3–2.0 Ga by differentiation from a slightly depleted mantle source (Taylor et al., 1992). Accordingly, the Birimian of Ghana is considered as part of a major Proterozoic (Eburnean) episode of juvenile crustal accretion which has been recognized in other surrounding areas in West Africa, where it has been dated at 2.2–2.1 Ga by Abouchami et al. (1990). On the basis of isotopic data and occasional presence of calc-alkaline andesite-dacite-rhyolite sequences, the Birimian volcanic belts mostly represent island arc complexes and some are external back-arc basins (Pohl & Carlson, 1993). The authors have indicated that the crustal shortening period of the Birimian involved a closure of an oceanic basin (located between the Man Shield and the Nigeria Craton) where multiple arc–arc collisions or, in the west, arc-continental platform collisions took place. It is believed that the modern paradigm of the Birimian situation is the compression of the Indonesian-Melanesian Archipelago and the intervening basins by the northward migration of the Australian Plate towards the Asian continent (Pohl & Carlson, 1993). On the basis of trace element geochemistry of the Birimian volcanic rocks and field observations, the Birimian greenstone belts were believed to have formed in oceanic island arc environments similar to those inferred for the Late Archaean Superior Craton (Sylvester & Attoh, 1992). Thus, the Birimian volcanic rocks probably originated as immature island arcs built on oceanic crust. It has also been observed that there exist similarities in regional geological patterns and relative internal age relationships between the Palaeoproterozoic Eburnean orogen of Ghana and the late Archaean Kenoran orogen of the southern Superior Province in Canada (Davis et al., 1994). In the southern Superior Province of Canada, deposition of volcanogenic-turbiditic basin sediments is suggested to be synchronous with accretion of arcs and micro-continental fragments against a growing continental mass. The authors have, therefore, proposed that the Birimian sedimentary basins resulted from accretion of arcs and oceanic plateaus now represented by allochthonous Birimian volcanic belts. Loh and Hirdes (1999), largely based on field observation, low TiO_2 contents as well as a calc-alkaline differentiation trend for basalts from the southern Ashanti belt, agree with Sylvester and Attoh (1992) that the Birimian rocks erupted in a primitive island-arc environment. When metagreywackes and metapelites from the Birim diamondiferous field were studied, they showed geochemical signatures similar to their Archaean counterparts (Asiedu et al., 2004). The chemical data of the rocks suggest that the rocks were derived from the basaltic to dacitic volcanic rocks and granItoids within the Birimian greenstone belts and were deposited in a tectonic setting comparable to modern island arcs (Asiedu et al., 2004). Furthermore, the geochemical signatures of the I-type granitoids from the southern Ashanti belt are consistent with those of granitoids emplaced in volcanic-arc settings (Dampare et al., 2005). Considering the fact that the belt granitoids and volcanic rocks of the Birimian terrane of Ghana are coeval (Davis et al., 1994; Hirdes et al., 1992), an island arc tectonic setting is inferred for the Birimian belts (Dampare et al., 2005). On the basis of metallogenesis model for the occurrence of gold deposits in Ghanam, a combination of continental margin, juvenile magmatism and convergence and collision between an old continent and a juvenile crust has been implied for the tectonic environments in which the Birimian greenstone belts were generated (Feybesse et al., 2006). The authors have stressed that the Ashanti volcanic belt marks the boundary between an Archaean continental domain and a Birimian oceanic domain. However, the results of numerical modelling using thermal parameters such as thermal conductivity values and heat-production rates led Harcouët, Guillou-Frottier, Bonneville, Bouchot, and Milesi (2007) to suggest that the basement in the Ashanti area is likely to be of continental rather than of oceanic type. Using field relationships, geochemistry, and the association of rodingite with the mafic–ultramafic complex in the southern Ashanti belt, the complex has recently been re-interpreted as a fragment of Palaeoproterozoic ophiolitic complex emplaced in a supra-subduction zone (SSZ) tectonic setting (Attoh et al., 2006). Also, an intra-oceanic island arc–fore-arc–back-arc setting is inferred for the Palaeoproterozoic metavolcanic rocks associated with the mafic–ultramafic complex (Dampare, Shibata, Asiedu, Osae, & Banoeng-Yakubo, 2008). Thus, interpretations of tectonic models for the Birimian terrane of Ghana basically varies between the intracratonic rift setting and island arc complexes.

The southern Ashanti volcanic belt follows the general geological disposition of the Ashanti belt, which is characterized by alternating NE–SW trending volcanic rocks and synvolcanic granitoids. The overall geological structural of the Ashanti belt is that of a synform, whereby the overlying Tarkwaian rocks occupy the centre of the belt and the Birimian volcanic rocks occur along the margins of the belt. The north-western margin of the Ashanti belt is strongly tectonized, represented by the Prestea–Obuasi–Konongo high-strain zone. The southern portion of the Ashanti volcanic belt forms three branches referred to as the Axim branch, Cape Three Point branch, and Butre branch, with three plutons (locally termed as Prince's Town, Dixcove, and Ketan pluton) occupying positions between these branches (Loh & Hirdes, 1999). The volcanic branches are composed of basaltic and andesitic lavas and pyroclastic rocks. The bulk of these andesitic rocks occur in the Axim volcanic branch where they probably occupy a stratigraphically upper position in the volcanic sequence of the southern Ashanti belt (Loh & Hirdes, 1999). The volcanic branches and the synvolcanic plutons are generally separated by normal faults/thrust zones. Several mafic–ultramafic rocks are associated with the volcanic rocks in the southern Ashanti volcanic belt (Figure 2). The age of the metavolcanic rocks is mainly constrained by the ages of the granitoids.

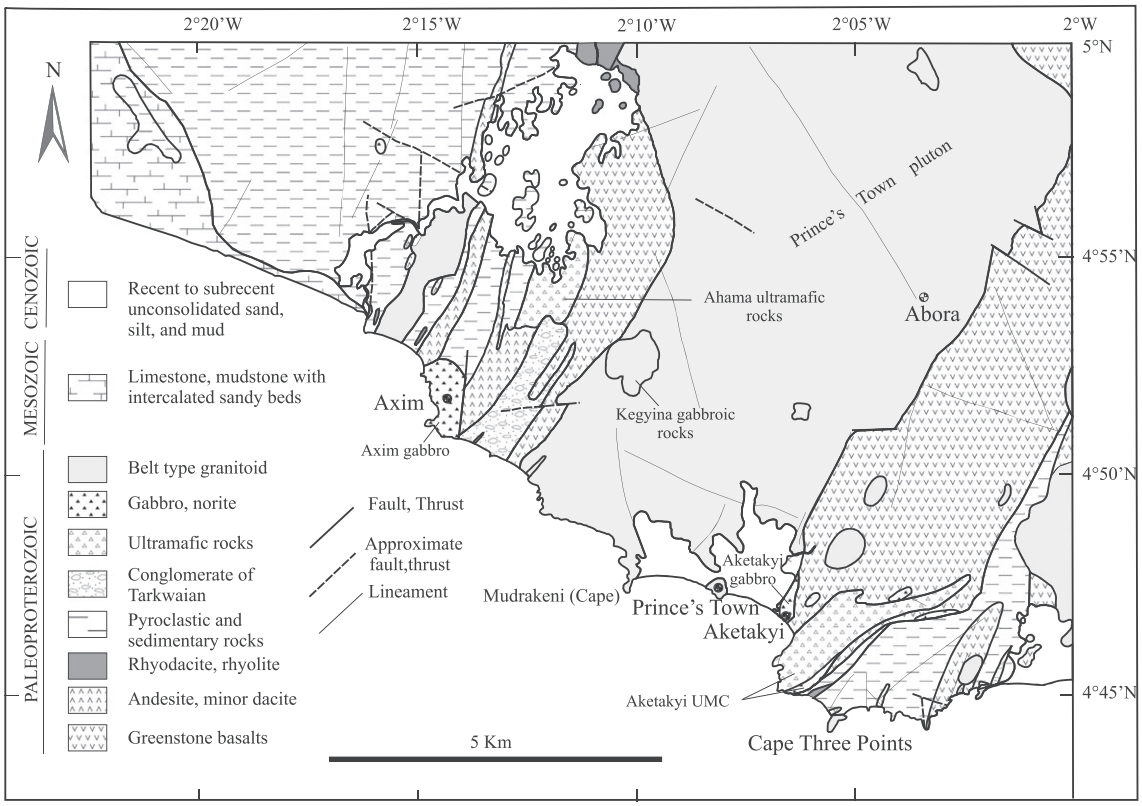

FIGURE 2 Geological map of the southern Ashanti volcanic belt of Ghana showing the Axim (left) and Cape Three Points (right) volcanic branches (after Loh & Hirdes, 1999)

The precise TIMS U–Pb zircon ages obtained for the migmatites and granitoids from the Ketan pluton, a tonalite from the Dixcove pluton, and a granodiorite from the Prince's Town pluton are 2,172 ± 4 Ma (Opare-Addo, John, Mukasa, & Browning, 1993), 2,174 ± 2 Ma (Hirdes et al., 1992) and 2,159 ± 4 Ma (Attoh et al., 2006), respectively. The age of the Prince's Town pluton has constrained a minimum age for the Aketakyi ophiolitic complex, as it intrudes the western flank of the complex.

2.2.2 | Birimian and pre-Birimian crust

Existing geochronological data to date appear to suggest two successive, major plutonism and volcanism episodes of Palaeoproterozoic crust formation in the West African Craton. These include the so-called Birimian sensu stricto (2,185–2,150 Ma, occurring in Ghana, eastern Cote d'Ivoire, and eastern part of Burkina Faso) and the so-called Bandamian (2,115–2,100 Ma, covering central and western Cote d'Ivoire, western Burkina Faso, Guinea, and Mali). Gasquet et al. (2003) obtained U–Pb ID-TIMS and SIMS zircon ages in the range of 2,103–2,162 Ma) and Nd model ages of 2,039–2,148 Ma for rocks from the Dabakala area of Cote d'Ivoire. An age of 2,312 ± 17 Ma was, however, obtained for zircon cores from the Dabakala tonalite, which also yielded an older Nd model age of 2,471 Ma. The authors interpreted this model age in the context of recycling of old 2.3 Ga material rather than the contribution of an ancient Archaean material due to the presence of 2,312 Ma old zircon cores and the low $^{87}Sr/^{86}Sr$ initial ratio of the rocks. Gasquet et al. (2003) suggested that the Birimian and Bandamian events were probably preceded by an early Palaeoproterozoic crustal growth event at ~2.3 Ga (Gasquet et al., 2003). The existence of a pre-Birimian event in the West African Craton is suggested by abundant geochronological and isotope geochemical data (e.g., Davis et al., 1994; Gasquet et al., 2003; Lemoine, 1988; Loh & Hirdes, 1999; Pawlig et al., 2006). Pawlig et al. (2006) demonstrated that this Early Birimian phase also occurred in the Kedougou-Kenieba-Inlier (KKI) of Eastern Senegal, which had previously been suggested to be among the youngest parts of the Birimian terrane (Hirdes et al., 1996; Hirdes & Davis, 2002). Thus, such an event is not limited to a particular region within the Palaeoproterozoic terrane of the WAC. Isotopic data also appear to suggest that the Eburnean orogeny represents a major juvenile crust-forming process with little or negligible involvement of an Archaean continental crust. The Winneba area and the vicinity of the Man nucleus have often been cited as the exceptional case, where a stronger influence of recycled Archaean basement is observed (e.g., Kouamelan, Peucat, & Delor, 1997; Taylor et al., 1992).

Taylor et al. (1992) carried out Rb–Sr, Pb/Pb, and Sm–Nd isotopic studies on selected Birimian metavolcanics, metasedimentary rocks and granitoids from Ghana. The absence of contamination in the igneous rocks, as indicated by the Sm/Nd ratios, led these authors to suggest that there was little evidence for the involvement of significantly older crust in the genesis of the volcanic-plutonic rocks. Taylor et al. (1992), therefore, discounted the possibility of an Archaean crust in

Ghana. Feybesse et al. (2006) held a contrary view; that is, the basic nature of the Palaeoproterozoic magmatism suggests a deep (i.e., mantle) origin and a very rapid rise, which probably accounted for the absence of contamination. The isotopic signature of the Winneba granitoids in south-eastern Ghana provides evidence of magmatic contribution from an older Archaean crust, which suggests that the Winneba area is probably underlain by an Archaean basement (Taylor et al., 1992). Other lines of evidence for the presence of an Archaean basement in Ghana include (a) the recent discovery of diamondiferous kimberlite in the Sunyani/Cape Coast Basin or the Akwatia and (b) the presence of end-Archaean to Siderian BIF-bearing supracrustal rocks in south-eastern Ghana (Feybesse et al., 2006). The authors suggested, therefore, that an Archaean basement probably exists below the Sunyani Basin and south-eastern Ghana, and that the Ashanti Belt could represent the boundary between an Archaean continental domain and a Birimian oceanic domain. The results of the numerical modelling, using thermal parameters such as thermal conductivity values and heat-production rates, suggest that the basement in the Ashanti area is likely to be of continental rather than of oceanic type (Harcouët et al., 2007). These authors supported the view that the lack of evidence of significantly older materials in Birimian rocks was probably due to the rapid nature of the ascending magma (e.g., Feybesse et al., 2006) rather than absence of continental basement, as suggested by Taylor et al. (1992).

3 | FIELD RELATIONS AND PETROGRAPHY

The field relations among the various rock types of the southern Ashanti volcanic belt are described in detail by Loh and Hirdes (1999), who indicated that the volcanic rocks form three major NE–SW trending lobes/branches referred to from east to west as the Butre branch, Cape Three Points branch, and the Axim branch. The volcanic branches are composed of basaltic and andesitic lavas, and pyroclastic rocks. The bulk of these andesitic rocks occur in the Axim volcanic branch where they probably occupy a stratigraphically upper position in the volcanic sequence of the southern Ashanti belt (Loh & Hirdes, 1999). Three granitoid intrusives, locally called the Prince's Town, Dixcove, and Ketan pluton, occur at intervening positions between the three major lobes/branches. Ultramafic to mafic complexes as well as isolated mafic bodies are associated with this greenstone–granitoid belt. The mafic and ultramafic rocks form a minor part of the entire intrusive bodies in the belt.

The study area is characterized by a major structural element, which is the high-strain zone to the north-west of Axim town in the belt/basin transition zone on the western flank of the Ashanti belt (Loh & Hirdes, 1999). This Axim high-strain zone is the southern continuation of the Prestea–Obuasi–Konongo high-strain zone, which hosts several major gold mines in Ghana. In this zone, sediments of the Kumasi Basin are thrust over the rocks of the Ashanti belt, including the Tarkwaian, in an oblique manner. Apart from the NE/NNE striking regional foliation, the several kilometre-wide Axim high-strain zone is characterized by numerous N–S shears, which are not prominently developed elsewhere in the belt (Loh & Hirdes, 1999). The effect of deformation in this high-strain zone is mainly observed in the incompetent argillitic sediments of the Kumasi Basin, whereas rocks within the Ashanti belt itself appear relatively undeformed (Loh & Hirdes, 1999).

3.1 | Prince's Town pluton

The Prince's Town granitoids have previously been studied by a number of workers including Loh and Hirdes (1999) and Dampare et al. (2005). The pluton consists of granitic to dioritic rocks, which are generally massive but occasionally display an alignment of ferromagnesian minerals. They are mostly greenish with pinkish tints and are typically medium-grained, but some of the granodiorites and the tonalites are coarse-grained. The mafic members (i.e., quartz diorites and diorites) tend to characterize the margins of the pluton, and the Prince's Town pluton is visualized as a single zoned magmatic intrusion (Loh & Hirdes, 1999). Thin section analysis indicates that the granitoids contain mainly plagioclase, K-feldspar, quartz, amphibole, biotite, and opaques. Accessory phases include zircon, apatite, and sphene. Plagioclase occurs as euhedral grains which display a variety of textures, including albite twinning and compositional zoning. Plagioclase is often sericitized and carbonated, and/or saussuritized, with the alteration being intense at the core. Fresh plagioclase crystals also occur in the rocks. K-feldspar partly displays a microperthitic to perthitic texture and is normally wrapped by euhedral plagioclase grains. Microcline is sericitized, carbonated, and/or saussuritized; fresh types are also present. In some of the rocks, feldspar exhibits a myrmekitic texture. The amphiboles are brownish-green in colour and have prismatic shapes and are partially altered to epidote and chlorite (Figure 3a). Biotite, mostly flaky, is often reddish-brown and is commonly altered to epidote and chlorite. Quartz is anhedral and displays undulatory extinction as well as sutured grained boundaries. Some of the quartz grains have been recrystallized and form fine-grained mosaics in the rocks. In the quartz diorites, quartz frequently occurs as interstitial grains between plagioclase crystals. Apatite mostly occurs as stubby-prismatic grains. Sphene and zircon are present as subhedral and euhedral crystals, respectively.

3.2 | Ultramafic rocks

The ultramafic–mafic rocks in the study area occur as two discrete bodies, that is, Aketakyi ultramafic complex (UMC) and Ahama ultramafic body.

3.2.1 | Aketakyi ultramafic complex

The Aketakyi UMC, which was previously mapped by Bartholomew (1961) and Loh and Hirdes (1999), has recently been re-interpreted as a fragment of Palaeoproterozoic ophiolitic complex by Attoh et al. (2006) based on geochemistry and the association of rodingite with the UMC. The rocks are well exposed on the coast and form a jagged coastline from Aketakyi to Cape Three Points, where they represent

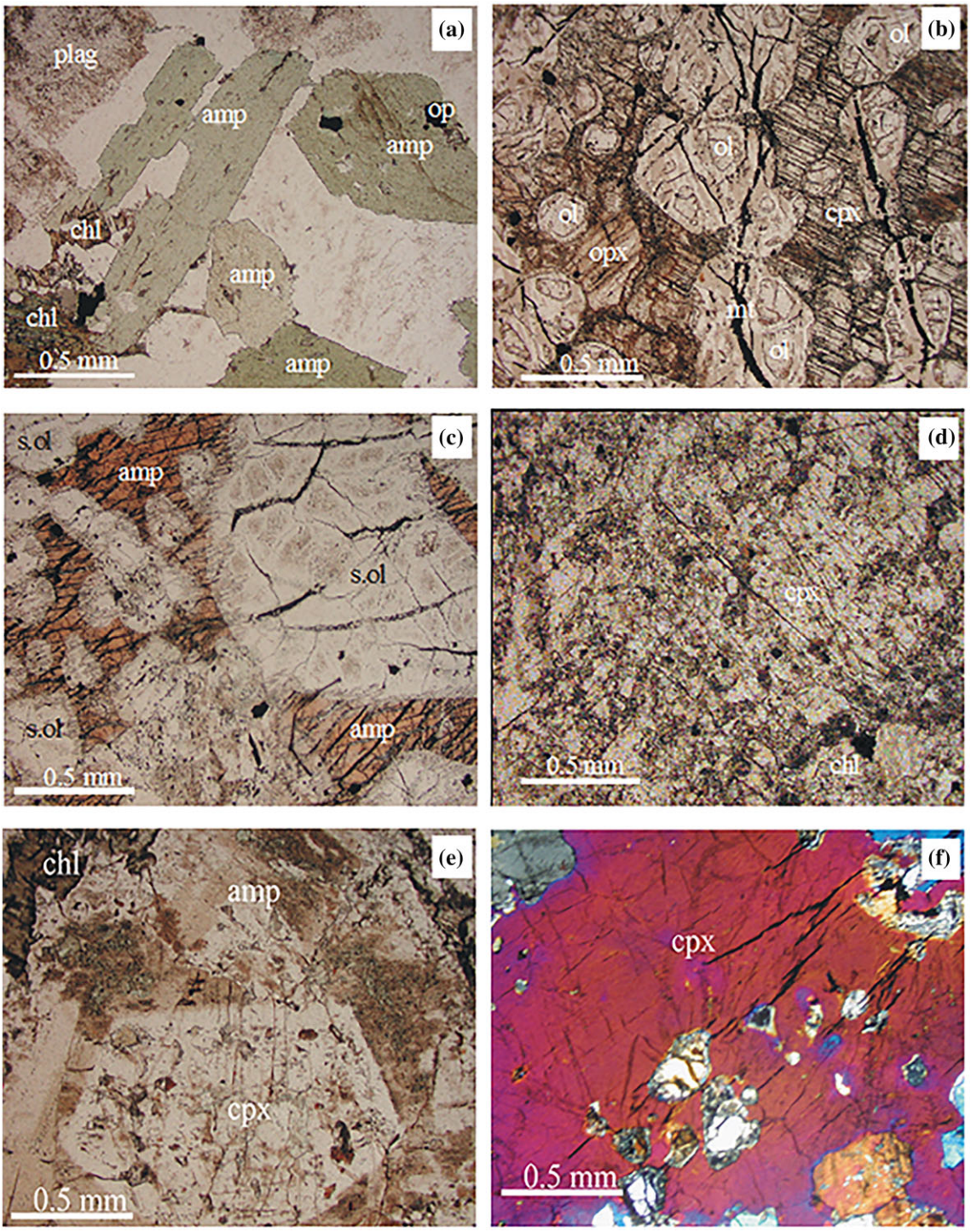

FIGURE 3 Photomicrographs of selected plutonic rocks from the study area: (a) Prince's Town granodiorite showing the occurrence of green amphibole (amp) in association with saussuritized plagioclase (plag); chlorite (chl) occurs as an alteration product of amphibole; Plane-Polarized Light. (b) Serpentinized peridotite of the Aketakyi ultramafic complex (UMC) showing relict olivine (ol) and orthopyroxene (opx) enclosed in a large clinopyroxene (cpx) crystal; Olivine is partly replaced by serpentine (ser). Plane-Polarized Light. Mt = magnetite. (c) Serpentinized peridotite of Aketakyi UMC showing brown amphibole (amp) oikocryst poikilitically enclosing serpentinized olivine (s.ol); Plane-Polarized Light. (d) Pyroxenite from the Ahama ultramafic-mafic body showing a large clinopyroxene crystal being replaced by chlorite; Plane-Polarized Light. (e) Axim gabbro showing relict clinopyroxene (cpx) which commonly forms the core of amphibole (amp) crystals; hornblende is partly replaced by chlorite. Plane-Polarized Light. (f) A typical large clinopyroxene (cpx) crystal in the Kegyina gabbro. Cross-Polarized Light [Colour figure can be viewed at wileyonlinelibrary.com]

the east central synclinal flank of the southern Ashanti volcanic belt. The western contact of the Aketakyi UMC is marked by fault and considered to represent the lower section of the complex, where it is made up of ~2.0-km-thick zone of coarse-grained peridotites, including harzburgite and dunite (Attoh et al., 2006). The rocks are variably serpentinized and altered to various degrees. Layering in the ultramafic complex appears to follow the regional north-east strike of the volcanic belt. This layering is more pronounced in the gabbroic rocks, which occur in the eastern contact zone. Rodingite occurs in the ultramafic rocks. Attoh et al. (2006) recognized the similarities between the Birimian rodingite occurrence in the Aketakyi UMC and those from ultramafic rocks of Archaean, including the Abitibi and Barberton greenstone belts, as well as the Phanerozoic rodingite occurrence in the ultramafic zones of ophiolitic complexes or modern oceanic crust. The protolith of the rodingites is uncertain.

The gabbroic zone of the ultramafic complex is stratigraphically overlain by a sheeted-dyke complex, which consists of basaltic hyaloclastites intercalated with fine-grained sediments including chert and disrupted basaltic-andesitic sills. A detailed description of the Aketakyi UMC is provided by Attoh et al. (2006). The ultramafic complex is associated with volcanic rocks. The volcanic pile consists of pillow breccias and hyaloclastites at the base, pillowed and massive lava flows in the middle, and aquagene tuffs interbedded with massive flows at the top, capped by a manganese-oxide and manganese-carbonate deposit (Sylvester & Attoh, 1992). The ultramafic complex with the overlying sheeted-dyke complex and associated volcanics has been suggested to represent a cross-section of a Palaeoproterozoic oceanic crust (Attoh et al., 2006).

Primary minerals in the Aketakyi UMC include olivine, pyroxene, and amphibole (Figure 3b). Olivine occurs as oval and subrounded crystals, which show a wide range of sizes. Olivine is commonly serpentinized. Few grains are preserved. Both brown and green amphiboles occur in the rocks. Brown oikocrysts occur in almost all the samples as a postcumulus phase, enclosing serpentinized olivine (Figure 3c) and sometimes pyroxene. Secondary minerals include actinolite, chlorite, and tremolite. Actinolite replaces pyroxene and chlorite partly replaces amphibole. Chromite and magnetite commonly occur in the rocks. Ilmenite occurs as anhedral minerals in some of the rocks.

3.2.2 | Ahama ultramafic body

The Ahama ultramafic body was first discovered and mapped by Loh and Hirdes (1999). It is located in the area of the headwaters of the Ahama stream in the Axim volcanic branch. The rocks are poorly exposed. Like the Aketakyi ultramafic complex, the emplacement of the Ahama ultramafic body appears to predate shearing which affected the Birimian terrane of Ghana around 2.1 Ga (Loh & Hirdes, 1999). The Ahama rocks are massive, coarse-grained, dark green, and are mostly weathered and show various degrees of serpentinization. The Ahama rocks are predominantly pyroxenites. Primary minerals are poorly preserved. Only few pyroxene grains were identified. Pyroxene shows sector zoning, and it is mostly replaced by talc. Actinolite occurs as a secondary mineral. Opaques are also abundant in them. Epidote occurs as single euhedral crystals and as a replacement product of plagioclase. Pyroxene is replaced by hornblende. In some of the rocks, pyroxene is replaced by chlorite (Figure 3d).

3.3 | Mafic rocks

The gabbroic rocks occur as minor bodies in the study area, and they include the Axim gabbro, Kegyina gabbro, and gabbroic rocks from the Aketakyi area. Although the gabbroic rocks have not been dated, they appear to have different origins as well as emplacement records. The Axim body is believed to have formed later than the granitoids, whereas the Kegyina gabbro could be coeval with the granitoids. The Aketakyi gabbro is inferred to have been emplaced earlier than the Prince's Town pluton, as the latter intrudes the western flank of the Aketakyi ultramafic complex, of which the Aketakyi gabbro is considered to be part. According to Loh and Hirdes (1999), most of the gabbroic rocks appear to predate the Eburnean tectono-thermal event.

3.3.1 | Axim gabbro

The Axim gabbro is associated with argillite and andesitic lavas in the transition zone between the Kumasi basin and the Ashanti belt. The rocks are massive and show various degrees of alteration. The Axim gabbroic rocks are equigranular, medium-grained, and consist of plagioclase, pyroxene, and hornblende. Plagioclase is commonly saussuritized. Relict pyroxenes usually form the cores of hornblende crystals (Figure 3e). This feature is considered to have developed during the late magmatic stage and is not a product of post-magmatic replacement. Hornblende is partly replaced by chlorite. Sphene coexists with an opaque mineral suspected to be ilmenite. Sulphides also occur in the rocks.

3.3.2 | Aketakyi and Kegyina gabbroic rocks

The gabbroic body, which intrudes the area north of Aketakyi town, is considered as an equivalent of the Kegyina gabbro. This body is made up of fine- to coarse-grained types. The Aketakyi gabbroic rocks are associated with the Aketakyi ultramafic complex, and they commonly occur as strongly foliated rocks at the outer flanks of the ultramafic complex. The ultrabasic nature of some analysed gabbroic rocks led Loh and Hirdes (1999) to suggest that the gabbroic rocks could be part of the main Aketakyi ultramafic complex. For Attoh et al. (2006), the gabbro rocks represent the upper section of the ultramafic complex.

The Kegyina gabbro is poorly exposed and deeply weathered. It is located within the Prince's Town pluton towards its margin and probably represents the mafic boarder of the Prince's Town pluton (Loh & Hirdes, 1999). The rocks are coarse-grained and massive.

In both the Kegyina and Aketakyi gabbros, green amphiboles coexist with pyroxenes (Figure 3f). Pyroxene is often replaced by amphibole. Plagioclase is commonly saussuritized. Epidote occurs in some of the samples. Chlorite also occurs as an alteration product of

TABLE 1 Major element abundances in the representative samples from the Prince's Town granitoid suite

Rock type	Granodiorite	Granodiorite	Tonalite	Quartz diorite	Quartz diorite	Quartz diorite	Quartz diorite	Granodiorite	Granodiorite
Sample No.	D9013A	D9013B	D9021	D9023A	D9024A	D9024B	D9024C	D9025	D9038
SiO_2 (wt.%)	66.26	67.09	65.69	61.61	63.74	63.78	62.17	69.62	67.11
TiO_2	0.34	0.34	0.33	0.36	0.36	0.37	0.37	0.27	0.37
Al_2O_3	15.25	15.42	15.82	15.98	15.91	15.75	15.66	15.53	14.25
Fe_2O_3[a]	3.55	3.63	3.86	5.63	5.51	5.57	5.68	3.06	4.16
MnO	0.07	0.08	0.08	0.11	0.11	0.11	0.11	0.06	0.08
MgO	2.03	2.01	2.02	2.67	2.68	2.80	2.83	1.51	2.11
CaO	3.70	3.64	3.84	5.51	5.34	5.20	5.62	3.26	3.42
Na_2O	4.43	4.19	4.67	3.66	3.87	3.67	3.53	4.69	3.88
K_2O	2.42	2.37	1.95	1.60	1.43	1.48	1.37	1.85	2.90
P_2O_5	0.12	0.12	0.13	0.11	0.11	0.12	0.12	0.10	0.11
LOI	1.58	1.59	1.46	2.12	2.08	2.24	2.13	1.25	1.75
Total	99.74	100.49	99.84	99.35	101.14	101.08	99.58	101.20	100.13
Mg#	53.08	52.31	50.92	48.39	49.03	49.92	49.68	49.39	50.06
A/CNK	0.92	0.96	0.95	0.9	0.91	0.92	0.89	0.99	0.91
V (ppm)			73	74				49	76
Cr			200	200				160	170
Co			13	13				27	13
Ni			90	80				80	70
Cu			40	20				20	40
Zn			60	50				50	50
Ga			20	16				20	16
Rb			55	77				46	75
Sr			667	380				655	366
Y			9.3	23.9				9.7	24.3
Zr			104	118				98	130
Nb			3.2	4				2.9	4
Cs			1.1	1.4				1.1	1.4
Ba			712	837				681	845
La			15.8	32.7				17.7	32.7
Ce			33.8	42.4				33.2	41.5
Pr			4	6.18				4.18	6.16
Nd			14.9	20.9				14.9	21.6
Sm			2.76	3.97				2.76	3.95
Eu			0.812	1.09				0.775	1.08
Gd			2.16	3.85				2.16	3.82
Tb			0.31	0.59				0.29	0.6
Dy			1.65	3.31				1.5	3.33
Ho			0.3	0.68				0.28	0.67
Er			0.9	2.07				0.8	2.08
Tm			0.134	0.303				0.121	0.306
Yb			0.95	1.95				0.83	1.96
Lu			0.148	0.303				0.13	0.31
Hf			2.8	3.3				2.6	3.5

(Continues)

TABLE 1 (Continued)

Rock type Sample No.	Granodiorite D9013A	Granodiorite D9013B	Tonalite D9021	Quartz diorite D9023A	Quartz diorite D9024A	Quartz diorite D9024B	Quartz diorite D9024C	Granodiorite D9025	Granodiorite D9038
Ta			0.29	0.35				2.66	0.4
Pb			12	9				9	11
Th			2.9	4.01				3.77	4.03
U			0.95	1.15				0.89	1.1

Note. Mg# = 100*(MgO/40.32)/({Fe_2O_3/79.85} + MgO/40.32); A/CNK = Molecular Al_2O_3/(CaO + Na_2O).

[a]Total iron as Fe_2O_3.

amphibole. Accessory minerals include apatite, ilmenite, and magnetite. Some varieties contain hornblende and plagioclase which are commonly replaced by chlorite and epidote, respectively. Sulphides are, however, abundant in the Aketakyi gabbros.

4 | WHOLE-ROCK COMPOSITIONS AND ISOTOPE GEOCHEMISTRY

The analytical techniques used for the major, trace, and Sr–Nd isotope analyses of samples collected from mafic, ultramafic, and granitoid outcrops associated with metavolcanic rocks in the Axim and Cape Three Points volcanic branches of the southern Ashanti greenstone belt have been provided in Appendix A.

4.1 | Major and trace element geochemistry

4.1.1 | Prince's Town pluton

The chemical compositions of the Prince's Town granitoids are given in Table 1. Although some of the analysed samples show variable effects of alteration, this is not pronounced and is not evident in the chemical data. In particular, the trace elements show systematic patterns reflecting petrogenetic processes, although we cannot rule out that some of the variations in K_2O, Na_2O, Ba, Rb, and Sr may be due to minor post-crystallization changes. The major element characteristics of the analysed granitoids have been discussed by Dampare et al. (2005). Accordingly, only a summary of these features is reported.

All the analysed samples from the Prince's Town pluton have SiO_2 content of 63.0–70.5 wt.%; TiO_2 of 0.27–0.38 wt.%; Al_2O_3 of 14.50–16.33 wt.%; total iron, as Fe_2O_3 of 3.10–5.80 wt.%; MnO of 0.06–0.11 wt.%; MgO of 1.53–2.89 wt.%; CaO of 3.30–5.74 wt.%; (Na_2O + K_2O) content of 5.01–6.96 wt.% and Na_2O/K_2O ratios from 1.34 to 2.70; and P_2O_5 of 0.10–0.13 wt.%. The Mg# of the rocks ranges from 53 to 48. The rocks may be classified as meta-aluminous, medium-K, calc-alkaline I-type granitoids (Dampare et al., 2005; this study). This confirms the findings of Loh and Hirdes (1999) that the Prince's Town pluton is largely meta-aluminous and calc-alkaline in character. Loh and Hirdes (1999) have, however, indicated that the Prince's Town pluton is zoned with a mafic rim, and these mafic rocks (i.e., quartz diorite and diorite) show some deviation from the calc-alkaline trend defined by the other rock types such as the granites, granodiorites, and tonalites. Although there appears to be some differences in the chemistry of the analysed quartz diorite, granodiorite, and tonalite (Table 1), we are unable to confirm Loh and Hirdes' (1999) assertion, probably due to relatively limited number of samples examined in this study.

The analysed granitoids have low REE abundances (ΣREE = 79–120 ppm). The chondrite-normalized REE patterns have concave-upward shapes with slight LREE enrichment (La_N/Sm_N = 3.70–5.34; La_N/Yb_N = 11.93–15.30) and weak negative to no Eu anomalies (Eu/Eu* = 0.85–1.02; Figure 4a). The granitoids show LREE enrichment patterns with minor negative and positive Eu anomalies and demonstrate enrichment in LILE relative to HFSE and in LREE relative to HREE, with Th–U trough, negative Nb (and Ta), and pronounced Ti anomalies, and spikes in Pb (and Sr; Figure 5a).

4.1.2 | Ultramafic rocks

The ultramafic rocks in the study area include the Aketakyi ultramafic complex and the Ahama ultramafic body. The chemical compositions of the ultramafic rocks (Tables 2 and 3) as well as the mafic rocks have been plotted on the SiO_2 versus FeO*/MgO diagram (Figure 6). Figure 6 also includes the chemical data of the mafic and ultramafic rocks provided in Loh and Hirdes (1999), and our data are comparable to that of Loh and Hirdes (1999). The rocks are mostly subalkaline and fall on both sides of the tholeiitic/calc-alkaline divide defined by Miyashiro (1974). Variations in the contents of major elements and selected trace elements with MgO are also shown in Figure 7.

Aketakyi ultramafic complex

Major and trace element data for the Aketakyi UMC are listed in Table 2. The analysed ultramafic–mafic rocks have SiO_2, (Na_2O + K_2O), MgO, and TiO_2 contents of 42.3–53.7 wt.%, 0.0–2.14 wt.%, 15.1–36.5 wt.%, and 0.09–0.61 wt.%, respectively. The Al_2O_3 (2.75–11.8 wt.%) and CaO (2.20–13.5 wt.%) contents in the rocks range from low to high values with the high values observed in the pyroxenitic and gabbroic rocks. The ultramafic–mafic rocks are characterized by moderate to high Mg numbers ranging from 72 to 84 with Ni contents of 710–1,650 ppm and Cr of 1,590–3,940 ppm (Table 2).

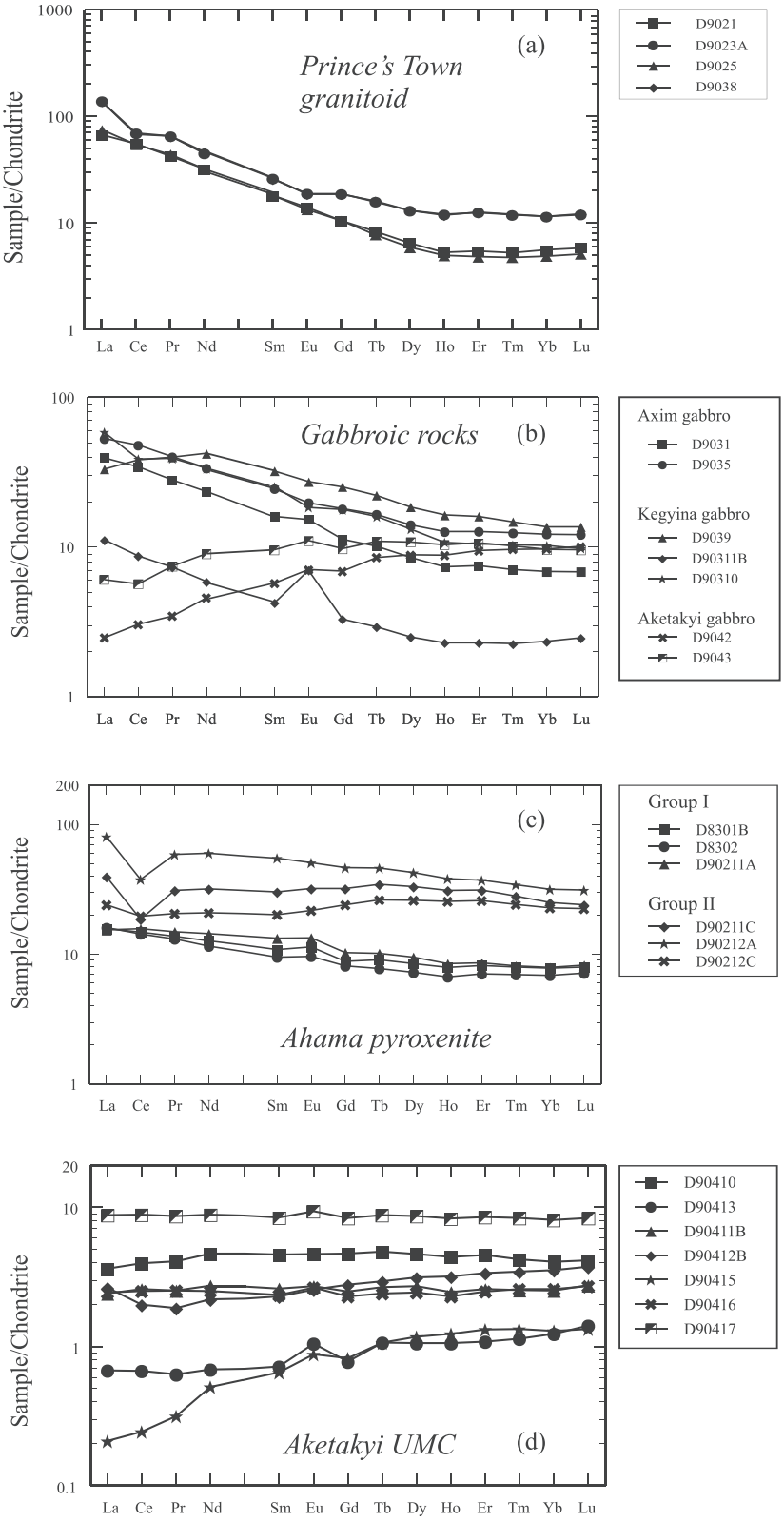

FIGURE 4 Chondrite-normalized patterns of plutonic rocks from the southern Ashanti greenstone belt: (a) Prince's Town granitoids, (b) Gabbroic rocks, (c) Ahama pyroxenites, and (d) Aketakyi ultramafic complex. Normalization values after Sun and McDonough (1989)

The high loss-on-ignition observed in these rocks resulted from serpentinization. Compositional variations in the ultramafic–mafic rocks are represented by a plot of major and trace elements versus MgO (Figure 7). The chemical compositions of the ultramafic–mafic rocks are plotted together with the previous chemical data of Loh and Hirdes (1999) in the Al_2O_3–CaO–MgO diagram of Coleman (1977; Figure 8). The analysed rocks fall in the fields of ophiolitic cumulate rocks.

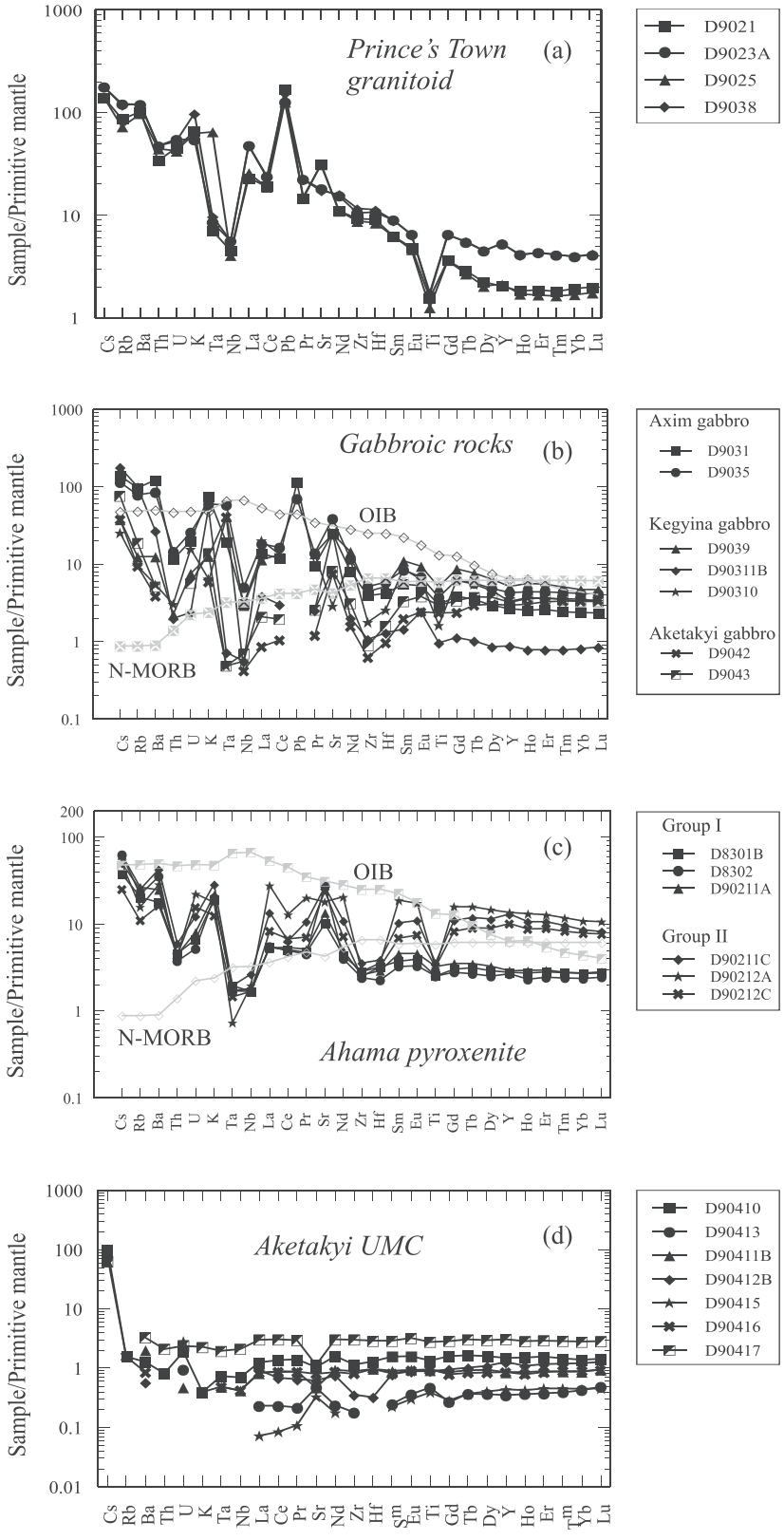

FIGURE 5 Primitive-mantle-normalized multi-element patterns of plutonic rocks from the southern Ashanti greenstone belt: (a) Prince's Town granitoids, (b) Gabbroic rocks, (c) Ahama pyroxenites, and (d) Aketakyi ultramafic complex. Normalization values, OIB, and N-MORB are from Sun and McDonough (1989)

The ultramafic–mafic rocks display LREE-depleted to flat, chondrite-normalized REE patterns ($(La/Sm)_N$ = 0.32–1.16; $(La/Yb)_N$ = 0.16–1.16) with no to minor positive Eu anomalies (Eu/Eu^* = 1.00–1.41) and with total REE contents ranging from 1.71 to 22.3 ppm (Figure 4d). The positive Eu anomalies observed in some of the rocks suggest that plagioclase was a cumulative phase in the formation of those rocks. On the primitive-mantle-normalized, trace element diagram, they show enrichment in Cs, slightly negative Th and Nb anomalies, and variable but minor positive and negative Sr, Hf, and Ti anomalies (Figure 5d).

TABLE 2 Representative whole-rock major and trace element chemical analyses of the Aketakyi ultramafic complex from the southern Ashanti volcanic belt

	AKT9 Hz	AKT10 Hz	D90410 Hz	D90413 Hz	D90416 Hz	D90411AD	D90411BD	AKT2AD	D9046 Py	D90412B Py	D90415 Py	D90417 Py	D90412G
SiO_2 (wt.%)	41.35	40.09	39.60	39.19	40.52	38.73	38.10	37.77	48.44	51.13	44.11	46.63	49.63
TiO_2	0.22	0.20	0.26	0.09	0.19	0.15	0.18	0.11	0.54	0.18	0.08	0.57	0.15
Al_2O_3	5.30	4.41	3.42	2.46	3.74	2.70	2.84	2.98	5.29	3.22	5.93	10.03	11.39
Fe_2O_3[a]	12.57	12.88	13.58	13.19	13.12	13.88	13.82	13.77	10.50	8.62	11.50	12.29	6.59
MnO	0.18	0.18	0.18	0.19	0.20	0.19	0.18	0.20	0.13	0.18	0.17	0.17	0.13
MgO	26.71	28.41	29.83	31.03	28.72	32.79	31.82	32.11	21.61	22.29	23.55	15.62	14.52
CaO	4.31	3.55	2.93	1.97	2.99	2.18	2.34	2.31	6.76	9.12	7.02	7.02	12.96
Na_2O	0.35	0.25	0.21	0.06	0.18	0.08	0.13	0.02	0.43	0.21	0.03	2.07	0.82
K_2O	0.03	0.02	0.01	0.00	0.01	0.00	0.00	0.00	0.03	0.00	0.00	0.07	0.01
P_2O_5	0.02	0.03	0.02	0.01	0.02	0.02	0.02	0.01	0.03	0.01	0.01	0.06	0.01
LOI	8.74	9.39	9.97	10.46	10.02	10.23	10.14	10.78	6.02	4.68	7.10	5.23	3.60
Total	99.79	99.43	100.01	98.65	99.71	100.95	99.57	100.07	99.77	99.65	99.50	99.77	99.82
Mg#	80.80	81.37	81.30	82.32	81.26	82.39	82.02	82.20	80.30	83.67	80.21	71.57	81.34
V (ppm)			105	61	86		80			129	81	223	
Cr			3,550	3,410	3,190		3,940			3,170	2,560	1,590	
Co			127	126	124		140			76	113	84	
Ni			1,510	1,500	1,450		1,650			710	1,170	740	
Cu			50	10	30		30			20	<10	100	
Zn			70	60	70		70			50	40	80	
Ga			5	4	6		4			5	6	12	
Rb			1	<1	1		<1			<1	<1	<1	
Sr			22	10	17		10			13	7	24	
Y			6.8	1.6	3.9		3.9			5.8	2	14	
Zr			13	2	9		10			4	<1	34	
Nb			0.5	<0.2	0.3		0.3			<0.2	<0.2	1.5	
Cs			0.8	0.6	0.6		0.5			<0.1	<0.1	0.5	
Ba			9	<3	6		14			4	<3	23	
La			0.86	0.16	0.58		0.57			0.63	0.05	2.09	
Ce			2.43	0.41	1.53		1.58			1.22	0.15	5.44	
Pr			0.39	0.06	0.24		0.24			0.18	0.03	0.82	
Nd			2.17	0.32	1.17		1.28			1.02	0.24	4.14	
Sm			0.7	0.11	0.36		0.4			0.35	0.1	1.29	
Eu			0.267	0.061	0.154		0.158			0.149	0.051	0.542	
Gd			0.96	0.16	0.47		0.51			0.57	0.17	1.72	
Tb			0.18	0.04	0.09		0.1			0.11	0.04	0.33	
Dy			1.17	0.27	0.62		0.69			0.8	0.3	2.19	
Ho			0.25	0.06	0.13		0.14			0.18	0.07	0.47	
Er			0.75	0.18	0.41		0.43			0.56	0.22	1.41	
Tm			0.108	0.029	0.066		0.065			0.088	0.034	0.213	
Yb			0.69	0.21	0.44		0.43			0.6	0.22	1.38	
Lu			0.106	0.036	0.069		0.07			0.095	0.034	0.212	

(Continues)

TABLE 2 (Continued)

	AKT9 Hz	AKT10 Hz	D90410 Hz	D90413 Hz	D90416 Hz	D90411A D	D90411B D	AKT2A D	D9046 Py	D90412B Py	D90415 Py	D90417 Py	D90412 G
Hf			0.4	<0.1	0.3		0.3			0.1	<0.1	0.9	
Ta			0.03	<0.01	0.02		0.02			<0.01	<0.01	0.08	
Pb			<5	<5	<5		<5			<5	<5	<5	
Th			0.07	<0.05	<0.05		<0.05			<0.05	<0.05	0.18	
U			0.04	0.02	<0.01		0.01			<0.01	0.06	0.05	

Note. Hz: Harzburgitite; D: Dunite; Py: Pyroxenite; G: Gabbro. Magnesium number (Mg#) = 100 × molar $Mg^{2+}/(Mg^{2+} + Fe^{2+})$.

[a]Total iron as Fe_2O_3.

Ahama ultramafic body (pyroxenites)

The chemical compositions of the Ahama pyroxenites are listed in Table 3. The LOI values of the ultramafic rocks in the study area (Ahama and Aketakyi rocks) are high due to alteration; microscopic studies also indicate that these are variably altered and serpentinized. In what follows, the major oxides of the rocks in data plots are presented on a volatile-free basis to reduce the effect of variable dilution resulting from serpentinization.

The Ahama pyroxenites have SiO_2, ($Na_2O + K_2O$), MgO, and TiO_2 contents of 48.7–50.5 wt.%, 1.30–2.81 wt.%, 7.98–12.6 wt.%, and 0.54–0.78 wt.%, respectively, and are characterized by low Mg numbers ranging from 63 to 74 with Ni contents of 170–520 ppm, and Cr of 630–1,580 ppm. The trace element geochemistry reveals two types of pyroxenites. The Group I pyroxenites show LREE enrichment patterns with $(La/Sm)_N$ = 1.16–1.70, $(La/Yb)_N$ = 1.94–2.34, minor positive Eu anomalies (Eu/Eu^* = 1.09–1.17), minor Ce anomalies of 0.98–1.03, and ∑REE contents of 28.1–32.8 ppm (Figure 4c). The Group II pyroxenites also show fractionated REE patterns with $(La/Sm)_N$ = 1.20–1.47, $(La/Yb)_N$ = 1.06–2.55, Eu anomalies of 0.99–1.03, significant negative Ce anomalies of 0.53–0.88, and relatively higher ∑REE contents of 57.1–124 ppm (Figure 4c). Both types of pyroxenites are characterized by enrichment in LILE relative to HFSE and in LREE relative to HREE. The Group I pyroxenites show Th–U and Nb–Ta troughs, positive Sr anomalies and minor negative Zr–Hf and Ti anomalies, whereas the Group II pyroxenites exhibit negative Th anomalies, pronounced negative Nb, Zr–Hf and Ti anomalies, and spikes in Sr (Figure 5c).

4.1.3 | Mafic rocks

Whole-rock compositions of the gabbroic intrusives in the southern Ashanti greenstone belt are presented in Table 4. The chemical compositions of the mafic and ultramafic rocks have been plotted on the SiO_2 versus FeO^*/MgO diagram (Figure 6). Figure 6 also includes the chemical data of the mafic and ultramafic rocks provided in Loh and Hirdes (1999), and our data are comparable to that of Loh and Hirdes (1999). The rocks are mostly subalkaline and fall on both sides of the tholeiitic/calc-alkaline divide defined by Miyashiro (1974). Variations in the contents of major elements and selected trace elements with MgO are also shown in Figure 7.

Axim gabbro

The analysed Axim gabbros have SiO_2, total alkalis ($Na_2O + K_2O$), high MgO, and low TiO_2 contents of 50.3–51.8 wt.%, 4.38–4.39 wt.%, 7.02–10.5 wt.%, and 0.65–0.82 wt.%, respectively. Their Mg numbers range from 54 to 68, and they have Ni and Cr contents of 140–250 and 340–880 ppm, respectively. The Axim gabbros exhibit slightly LREE-enriched patterns, $(La/Sm)_N$ = 2.16–2.46 and $(La/Yb)_N$ = 4.35–5.76, with minor negative and positive Eu anomalies (Eu/Eu^* = 0.94–1.14; Figure 4b). Primitive-mantle-normalized, trace element patterns show that the gabbros have geochemical patterns characterized by enrichment in LILE (e.g., Cs, Rb, and Ba) relative to HFSE (e.g., Nb, Zr, Hf, Ta, Ti, and Y) and in LREE relative to HREE, with Th–U trough, pronounced negative Nb anomalies, negative Zr–Hf and Ti anomalies, and spikes in Pb and Sr (Figure 5b).

Kegyina gabbro

The Kegyina gabbroic rocks have SiO_2, ($Na_2O + K_2O$), MgO, and TiO_2 contents of 48.1–52.6 wt.%, 0.83–4.78 wt.%, 4.88–15.4 wt.%, and 0.21–1.10 wt.%, respectively, and Mg numbers of 63–74, Ni contents of 170–520 ppm and Cr of 630–1,580 ppm. The rocks commonly show LREE enrichment patterns with $(La/Sm)_N$ = 1.03–2.64, $(La/Yb)_N$ = 2.43–5.70, and minor negative to strong positive Eu anomalies (Eu/Eu^* = 0.87–1.87). Sample D9039 (isolated massive gabbro from Kegyina) shows a convex-upward REE pattern which is typical of pyroxene-dominated cumulates (McDonough & Frey, 1989) with the apex at Nd (McDonough & Frey, 1989; Figure 4b). On the primitive-mantle-normalized, trace element diagram, the gabbroic rocks show enrichment in LILE relative to HFSE and in LREE relative to HREE with negative Th (and U), Nb (and Ta), Zr–Hf and Ti anomalies, and negative and positive Sr anomalies (Figure 5b)

Aketakyi gabbroic rocks

The analysed Aketakyi gabbroic rocks (i.e., those from the northern part of Aketakyi town) have SiO_2, ($Na_2O + K_2O$), MgO, and TiO_2 contents of 45.1–50.1 wt.%, 0.50–3.79 wt.%, 6.81–5.81 wt.%, and 0.49–0.99 wt.%, respectively. The Mg numbers range from 56 to 73, and their Ni and Cr contents are 160–430 and 270–440 ppm, respectively. They show LREE-depleted patterns with $(La/Sm)_N$ = 0.43–0.63 and $(La/Yb)_N$ = 0.25–0.63 (Figure 4b). The gabbroic rocks are characterized by enrichment in LILE relative to HFSE, negative Zr–Hf and Ti anomalies, pronounced negative Nb and Ta anomalies and spikes in Sr (Figure 5b).

TABLE 3 Whole-rock major and trace element chemical analyses of the Ahama pyroxenitic rocks from the southern Ashanti volcanic belt

	D8301A	D8301B	D8301C	D8302	D90211A	D90211B	D90211C	D90212A	D90212B	D90212C
SiO_2 (wt.%)	47.11	47.44	47.30	47.80	46.63	46.56	47.36	47.07	46.35	47.67
TiO_2	0.54	0.51	0.55	0.52	0.67	0.69	0.74	0.64	0.68	0.68
Al_2O_3	9.78	9.23	9.83	10.18	9.53	9.51	11.51	9.47	8.93	9.89
Fe_2O_3[a]	10.39	10.61	10.16	10.18	11.69	11.97	11.95	11.93	12.21	12.38
MnO	0.17	0.17	0.16	0.16	0.20	0.20	0.19	0.19	0.21	0.20
MgO	15.00	15.49	14.59	14.45	12.45	12.54	10.37	12.52	12.80	12.62
CaO	7.50	7.88	7.57	8.36	11.88	11.06	10.28	11.79	12.00	12.24
Na_2O	1.75	1.60	1.80	1.83	1.01	1.01	1.49	1.07	0.93	1.11
K_2O	0.80	0.54	0.84	0.58	0.63	0.52	0.83	0.51	0.31	0.37
P_2O_5	0.16	0.14	0.16	0.14	0.17	0.17	0.20	0.16	0.17	0.17
LOI	6.00	6.12	6.08	5.24	4.69	5.52	4.88	4.52	4.79	2.66
Total	99.21	99.74	99.03	99.43	99.53	99.77	99.79	99.89	99.38	100.00
Mg#	74.10	74.30	73.98	73.75	67.85	67.47	63.23	67.51	67.47	66.87
V (ppm)		187		195	214		241	227		221
Cr		1,490		1,580	810		630	830		760
Co		60		60	54		56	63		58
Ni		520		480	180		170	200		190
Cu		50		60	60		70	60		70
Zn		70		50	70		100	70		80
Ga		12		12	12		15	13		13
Rb		13		14	17		16	10		7
Sr		214		584	285		571	381		502
Y		12.7		12.2	13.3		59.3	62.3		46
Zr		32		27	29		40	32		28
Nb		1.2		1.2	1.3		1.9	1.4		1.2
Cs		0.3		0.5	0.5		0.4	0.4		0.2
Ba		124		248	174		300	201		114
La		3.73		3.81	3.66		9.34	19.1		5.71
Ce		9.06		8.75	9.61		11.4	23		12
Pr		1.31		1.25	1.42		2.95	5.57		1.96
Nd		5.93		5.4	6.73		14.9	27.9		9.77
Sm		1.66		1.45	2.04		4.61	8.38		3.08
Eu		0.662		0.557	0.774		1.86	2.93		1.26
Gd		1.81		1.67	2.11		6.6	9.51		4.93
Tb		0.34		0.29	0.38		1.29	1.72		0.98
Dy		2.15		1.85	2.41		8.43	10.8		6.6
Ho		0.45		0.38	0.48		1.76	2.16		1.44
Er		1.36		1.17	1.42		5.15	6.13		4.28
Tm		0.204		0.178	0.207		0.716	0.875		0.615
Yb		1.33		1.17	1.35		4.24	5.37		3.87
Lu		0.203		0.182	0.209		0.609	0.795		0.569
Hf		1		0.7	0.9		1.2	1.1		1
Ta		0.08		0.07	0.07		0.08	0.03		0.06
Pb		<5		<5	<5		<5	<5		<5

(Continues)

TABLE 3 (Continued)

	D8301A	D8301B	D8301C	D8302	D90211A	D90211B	D90211C	D90212A	D90212B	D90212C
Th		0.39		0.32	0.38		0.51	0.37		0.37
U		0.14		0.11	0.17		0.26	0.47		0.33

Note. Magnesium number (Mg#) = 100 × molar $Mg^{2+}/(Mg^{2+} + Fe^{2+})$.

[a]Total iron as Fe_2O_3.

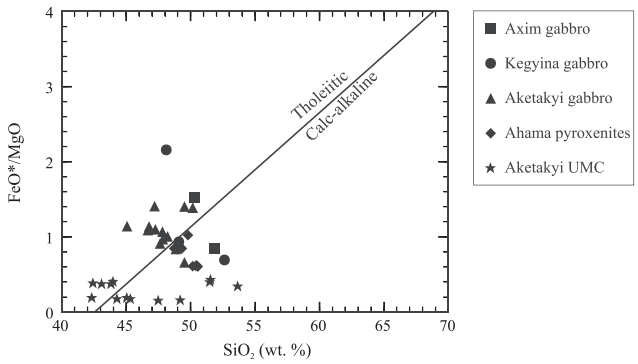

FIGURE 6 SiO_2 vs. FeO*/MgO diagram for the mafic–ultramafic plutonic rocks from the southern Ashanti greenstone belt. Previous chemical data of Loh and Hirdes (1999) have been included in the plot

4.2 | Sr–Nd isotopic data

Sr–Nd isotopic data, $^{87}Sr/^{86}Sr$ initial ratios, ε_{Nd} (T), and Nd model ages (T_{DM1} and T_{DM2}) are presented in Table 5. The initial $^{87}Sr/^{86}Sr$ ratios and ε_{Nd} values were calculated at an age of 2.1 Ga, which represents the crustal formation time during the Eburnean orogeny (e.g., Abouchami et al., 1990; Boher et al., 1992). The initial isotopic ratios were derived using Rb/Sr and Sm/Nd ratios from the ICP-MS data.

The rocks display low $^{87}Sr/^{86}Sr$ initial ratios (0.693178–0.702423). The low $^{87}Sr/^{86}Sr$ initial values of D9023A (0.693178) and D9038 (0.699468) probably suggest alteration of feldspar. The Sr initial ratios values are comparable to those previously reported on the Birimian basaltic and granitic rocks of West Africa (e.g., Abouchami et al., 1990; Boher et al., 1992; Gasquet et al., 2003; Taylor et al., 1992). These data show the primitive isotopic Sr signature of the rocks, thereby precluding significant magmatic contributions from Rb-enriched continental crust. The granitoids show a range of initial ε_{Nd} values from −1.01 to +2.92 at 2.1 Ga. The gabbros have initial ε_{Nd} (T) of −1.23 to +5.23. The Ahama pyroxenites show negative initial ε_{Nd} (T) values from −0.58 to −5.68. The meta-peridotites from the Aketakyi ultramafic/ophiolitic complex show high positive ε_{Nd} (T) values from +3.69 to +4.93.

Crustal residence ages (T_{DM}) may be calculated using diverse models of depleted mantle evolution. Nd models give ages which vary by several hundreds of Ma on the basis of previous studies (Albarède & Brouxel, 1987; Ben Othman et al., 1984; DePaolo, 1981; Goldstein, O'Nions, & Hamilton, 1984; McCulloch, 1987; Nelson & DePaolo, 1985). The model of Ben Othman et al. (1984) is considered to be representative of the Birimian depleted mantle (Abouchami et al., 1990) and was subsequently adopted by some workers including Abouchami et al. (1990), Boher et al. (1992), and Gasquet et al. (2003). However, following the approach of some earlier workers in the Birimian terrane of Ghana, one-stage model ages (T_{DM1}) have been calculated for the rocks, using the model of DePaolo (1981). The Nd model age of crustal rocks indicates their time of extraction from the mantle. However, the assumption that a Sm–Nd model age represents an average crustal residence time is valid only if no fractionation of Sm/Nd has taken place since the first separation of its protolith from the mantle source. This is, however, not always the case. In order to minimize the bias as a result of Sm/Nd fractionation, which might lead to either underestimation or overestimation of one-stage Nd model ages, a two-stage Nd model age (T_{DM2}) may be calculated for the rocks. The two-stage model age was computed following the procedure of Keto and Jacobsen (1987), and using the expression below:

$$T_{DM2} = T_{DM} - (T_{DM1} - t)\,[(f_{cc} - f_s)/(f_{cc} - f_{DM})],$$

where f_{cc}, f_s, and f_{DM} are the $f_{Sm/Nd}$ values of the continental crust, the sample, and depleted mantle, respectively, and t is the formation age of the rock; and $f_{Sm/Nd}$ is given by the expression:

$$f_{Sm/Nd} = \left[\left(^{147}Sm/^{144}Nd_{Sample}\right)/\left(^{147}Sm/^{144}Nd_{CHUR}\right)\right] - 1.$$

In this calculation, f_{cc} = −0.4, f_{DM} = 0.086426, and t = 2.1 Ga.

It is difficult to choose between one-stage and two-stage model ages as each has its own uncertainties (e.g., DePaolo, Linn, & Schubert, 1991; Wu, Zhao, Simon, Wilde, & Sun, 2005). Wu et al. (2005) indicated that more accurate results could be obtained for the single-stage model age, if the Sm/Nd fractionation, expressed as $f_{Sm/Nd}$, is limited to the range of −0.2 to −0.6.

In this study, the two-stage Nd model age (T_{DM2}) is preferred to the single-stage model age (T_{DM1}) as it displays a more regular pattern. The model ages are 2.12–2.45 Ga for the granitoids and 2.03–2.47 Ga for the gabbros. The Group I pyroxenites yielded T_{DM2} values of 2.43 to 2.61 Ga, whereas no meaningful Nd model ages were obtained for the Group II pyroxenites, as they yielded extremely high T_{DM} values. The analysed meta-peridotite samples from the Aketakyi ophiolitic complex yielded Nd model ages of 1.96 to 2.01 Ga.

5 | DISCUSSION

5.1 | Alteration effects

The rocks of the southern Ashanti greenstone belt have experienced peak amphibolite facies to retrograde greenschist-facies metamorphism, and mobility of some elements may have occurred. Alteration

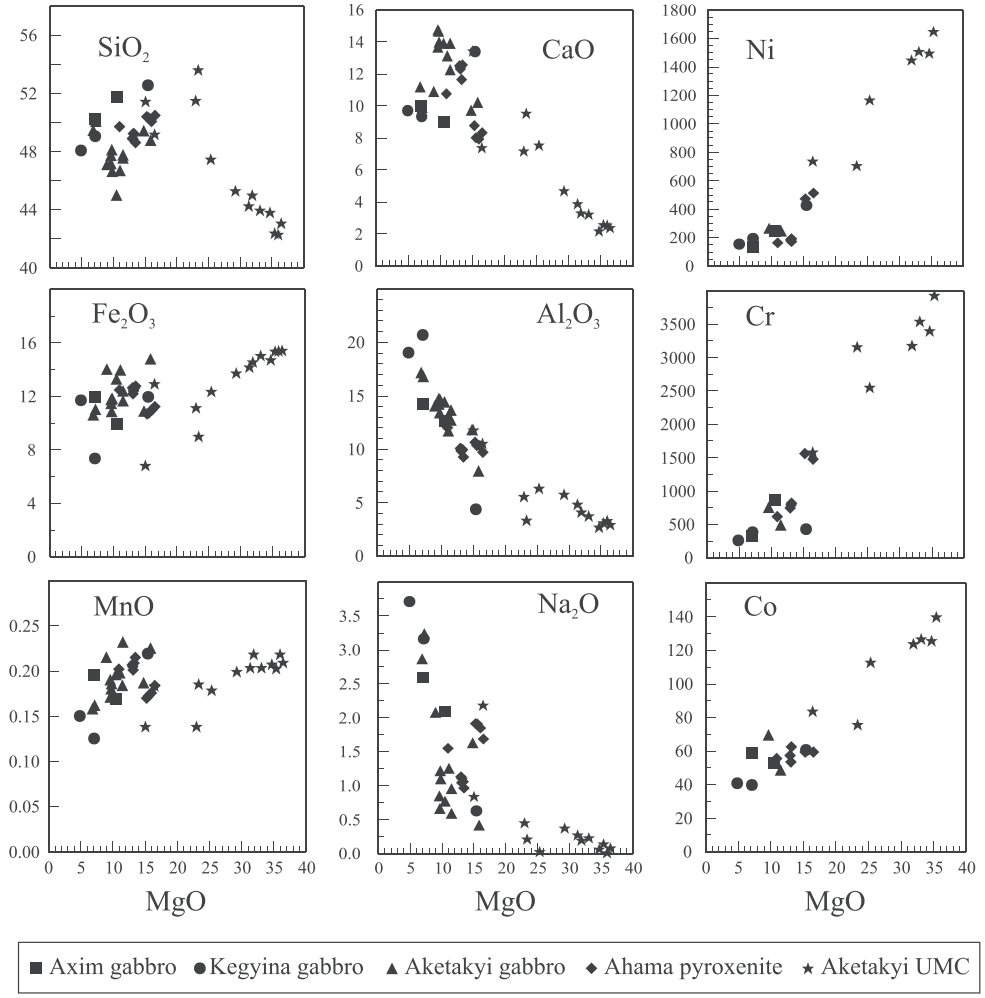

FIGURE 7 Selected major (wt.%) and trace elements (ppm) variations with MgO (wt.%) for the analysed mafic–ultramafic rocks in this study and that of Loh and Hirdes (1999)

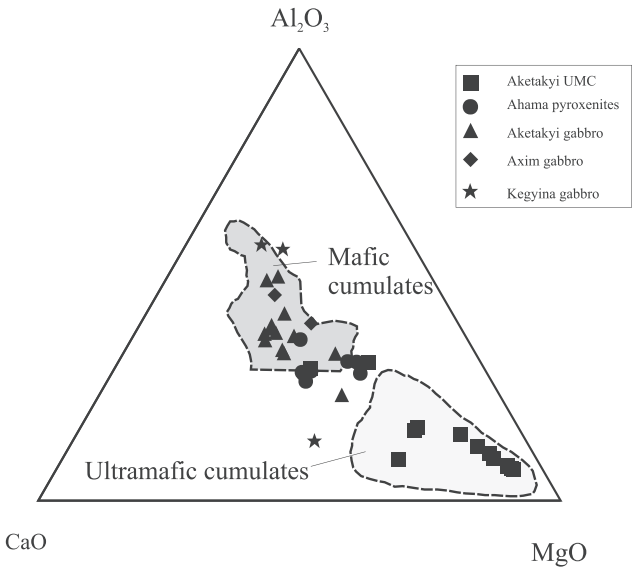

FIGURE 8 Al_2O_3–CaO–MgO plot of the mafic–ultramafic rocks compared with ophiolitic rocks (fields after Coleman, 1977). Loh and Hirdes' (1999) data have also been plotted

of plutonic rocks is a common phenomenon, especially in older rocks. It is usually evidenced by high loss-on-ignition (LOI) values and increased scatter and mobility of major and large-ion lithophile elements (LILE). Some studies have noted, however, that even for rocks of ancient heritage, the concentrations of such "mobile" elements are commonly not significantly changed from their primary abundances (e.g., Whalen, Syme, & Stern, 1999). The extent of alteration of rocks could also be investigated using the chemical index of alteration (CIA) calculations of Nesbitt and Young (1982). The CIA is defined as molar ($100^*Al_2O_3/(Al_2O_3 + CaO^* + Na_2O + K_2O)$), where CaO^* is the contribution of CaO from silicates only. According to Nesbitt and Young (1982), the CIA values for unaltered granite and basic rock are 50 and 42, respectively, while a CIA value of any rock exceeding 60 indicates a significant alteration. Therefore, rocks with less CIA values could be used for petrogenetic interpretations. Owing to the relatively immobile nature of HFSE and REEs under most conditions (e.g., Whalen et al., 1999), they have often been used for igneous petrogenetic and tectonic studies. Major elements have mostly been used to give background information due to their high susceptibility to mobility during processes such as metamorphism and

TABLE 4 Representative whole-rock major and trace element chemical analyses of the Palaeoproterozoic mafic rocks from the southern Ashanti volcanic belt

	Aketakyi gabbroic rocks								
	D9042[a]	D9043[a]	D9044[a]	AKT 2[a]	AKT 3[a]	AKT 4[a]	AKT 5[a]	AKT 6[a]	AKT 7[a]
SiO_2 (wt.%)	45.73	45.80	45.30	46.35	45.60	45.16	43.19	44.99	47.94
TiO_2	0.49	0.62	0.95	0.47	0.47	0.76	0.50	0.52	0.54
Al_2O_3	14.20	12.32	13.56	12.99	13.11	11.37	13.88	14.15	16.68
Fe_2O_3[b]	11.01	11.27	13.53	10.51	11.87	13.54	12.79	11.49	10.31
MnO	0.16	0.18	0.21	0.17	0.22	0.19	0.19	0.18	0.15
MgO	9.18	11.03	8.60	9.32	10.95	10.66	10.03	9.41	6.59
CaO	13.12	13.41	10.50	14.14	11.73	12.71	13.37	13.52	10.87
Na_2O	0.64	0.58	2.01	1.18	0.92	1.22	0.75	1.07	2.79
K_2O	0.17	0.40	0.28	0.20	0.11	0.20	0.09	0.11	0.46
P_2O_5	0.04	0.04	0.07	0.05	0.04	0.09	0.04	0.07	0.20
LOI	4.30	3.79	3.94	3.78	4.63	3.38	4.12	3.60	3.17
Total	99.05	99.43	98.95	99.17	99.65	99.27	98.95	99.10	99.71
Mg#	62.27	65.96	55.71	63.73	64.63	60.92	60.83	61.85	55.86
V (ppm)	246	292							
Cr	770	500							
Co	70	49							
Ni	270	250							
Cu	60	40							
Zn	60	60							
Ga	12	11							
Rb	6	12							
Sr	158	173							
Y	13.4	14.8							
Zr	7	10							
Nb	0.3	0.5							
Cs	0.3	0.6							
Ba	27	36							
La	0.59	1.44							
Ce	1.87	3.49							
Pr	0.33	0.71							
Nd	2.15	4.22							
Sm	0.88	1.47							
Eu	0.411	0.643							
Gd	1.42	2.01							
Tb	0.32	0.41							
Dy	2.26	2.76							
Ho	0.5	0.59							
Er	1.57	1.77							
Tm	0.247	0.26							
Yb	1.66	1.64							
Lu	0.257	0.244							
Hf	0.3	0.5							

(Continues)

TABLE 4 (Continued)

	Aketakyi gabbroic rocks								
	D9042[a]	D9043[a]	D9044[a]	AKT 2[a]	AKT 3[a]	AKT 4[a]	AKT 5[a]	AKT 6[a]	AKT 7[a]
Ta	1.67	0.02							
W	50.7	0.8							
Pb	<5	<5							
Th	<0.05	<0.05							
U	<0.01	0.12							

	Aketakyi gabbroic rocks				Axim gabbroic rocks		Kegyina gabbroic rocks		
	AKT 8[a]	AKT 12[a]	AKT 13[a]	AKT 14[a]	D9031[a]	D9035[a]	D9039[a]	D90310[a]	D90311B[a]
SiO_2 (wt.%)	45.36	46.29	48.33	47.48	49.83	48.57	46.41	51.02	47.45
TiO_2	0.46	0.63	0.65	0.57	0.62	0.79	1.06	0.34	0.20
Al_2O_3	13.74	7.62	16.29	11.44	12.24	13.85	18.44	4.29	20.05
Fe_2O_3[b]	11.35	14.08	10.69	10.52	9.59	11.58	11.32	11.65	7.17
MnO	0.18	0.21	0.16	0.18	0.16	0.19	0.15	0.21	0.12
MgO	9.20	14.98	6.90	14.17	10.12	6.78	4.71	14.96	6.85
CaO	14.20	9.73	9.58	9.37	8.72	9.66	9.39	13.02	9.06
Na_2O	0.83	0.41	3.13	1.57	2.03	2.51	3.59	0.62	3.06
K_2O	0.02	0.06	0.52	0.51	2.19	1.73	0.37	0.19	1.56
P_2O_5	0.04	0.06	0.26	0.05	0.27	0.28	0.25	0.03	0.03
LOI	3.96	5.21	3.61	4.07	3.76	3.42	3.50	2.99	3.32
Total	99.33	99.29	100.12	99.92	99.54	99.35	99.19	99.32	98.86
Mg#	61.63	67.81	56.10	72.74	67.64	53.70	45.17	71.78	65.44
V (ppm)					201	291	211	188	99
Cr					880	340	270	440	390
Co					53	59	41	61	40
Ni					250	140	160	430	200
Cu					130	70	80	290	40
Zn					70	80	90	< 30	50
Ga					14	18	20	7	20
Rb					61	50	8	6	63
Sr					532	815	520	61	538
Y					12.1	19.5	23.4	15	4
Zr					44	58	50	20	12
Nb					2.2	3.6	2.1	0.4	0.4
Cs					1.1	0.9	0.3	0.2	1.4
Ba					857	596	88	38	189
La					9.39	12.6	7.9	13.9	2.66
Ce					21.1	29.4	23.5	23.8	5.36
Pr					2.67	3.82	3.81	3.73	0.7
Nd					11	15.8	19.8	15.7	2.75
Sm					2.46	3.76	4.94	3.88	0.65
Eu					0.89	1.15	1.59	1.07	0.407
Gd					2.32	3.72	5.2	3.67	0.68
Tb					0.38	0.62	0.83	0.6	0.11

(Continues)

TABLE 4 (Continued)

	Aketakyi gabbroic rocks				Axim gabbroic rocks		Kegyina gabbroic rocks		
	AKT 8[a]	AKT 12[a]	AKT 13[a]	AKT 14[a]	D9031[a]	D9035[a]	D9039[a]	D90310[a]	D90311B[a]
Dy					2.17	3.59	4.71	3.36	0.64
Ho					0.42	0.72	0.93	0.61	0.13
Er					1.25	2.11	2.66	1.74	0.38
Tm					0.181	0.318	0.378	0.265	0.058
Yb					1.17	2.08	2.33	1.75	0.4
Lu					0.174	0.309	0.348	0.249	0.063
Hf					1.3	1.8	1.6	0.8	0.4
Ta					0.78	2.39	1.7	0.02	0.03
W					27.5	68	50.8	1.5	1.2
Pb					8	5	<5	<5	<5
Th					0.99	1.23	0.19	0.26	0.17
U					0.42	0.54	0.16	0.33	0.05

Note. Magnesium number (Mg#) = 100 × molar $Mg^{2+}/(Mg^{2+} + Fe^{2+})$.

[a]Sample.

[b]Total iron as Fe_2O_3.

hydrothermal activities. However, if the mobility of major elements is minimal, they could still reflect the primary igneous processes involved in the formation of the rocks. Although crustal reworking can result in inherited chemical signatures, it is less a problem here as isotopic character of the rocks is largely juvenile.

The analysed gabbroic rocks show variable alteration with LOI values ranging from 3.0 to 5.2 wt.%. Al; Ca; Mg; high-field-strength elements (HFSE) such as Th, Zr, Hf, Nb, Ta, Ti, Y; and REE may have remained immobile (e.g., Barnes et al., 1985). Potassium and rubidium may be easily changed during alteration; however, their nearly constant K_2O/Rb ratios (298–478) indicate that their original chemical compositions were not significantly modified. The CIA values for the gabbros range from 15 to 46 and that of Prince's Town rocks range from 47 to 50, indicating minimum alteration. Hence, geochemical compositions of the gabbroic rocks can approximately reflect their source characteristics. The LOI values of the ultramafic rocks are high due to alteration; microscopic studies also indicate that these rocks are variably altered and serpentinized. The low CIA values of the Ahama pyroxenite (27–36) and the Aketakyi UMC (16–41) suggest that they have not been severely altered. In what follows, the major oxides of the rocks in data plots are presented on a volatile-free basis to reduce the effect of variable dilution resulting from serpentinization. Also, we have mainly used the relatively immobile elements (HFSE, REE, and transition elements) in our interpretations.

5.2 | Petrogenesis

5.2.1 | Prince's Town pluton

The Prince's Town granitoids form part of the Dixcove- (or belt-type) granitoids of Ghana, which are metaluminous, Na-rich, dominantly hornblende- to biotite-bearing granodiorite to diorite, monzonite and syenite. Generally, the Palaeoproterozoic granitoids intruding the Birimian terrane of the Leo-Man Shield have been classified into two main groups according to the presence or absence of amphibole (Lompo, 2009 and references therein): (a) the amphibole-bearing granitoids (PAG) and (b) the biotite ± muscovite-bearing granitoids without amphibole (PBG). The Dixcove-type granitoids may be included in the PAG-type granitoids in the Birimian terrane.

Following the approach of Altherr et al. (2000) and using molar ratios of $CaO/(MgO + FeO_{tot})$ and $Al_2O_3/(MgO + FeO_{tot})$, Dampare et al. (2005) indicated that the granitoids were likely derived from partial melting of metaplutonic or metavolcanic rocks, possibly with a contribution from metagreywacke. The trace element data of the Prince's Town granitoids are broadly similar to the sodic calc-alkaline Birimian granitoids (NaCG) reported from central Cote d'Ivoire (Doumbia et al., 1998; Figure 9). Doumbia et al. (1998) suggested that NaCG may have been generated from partial melting of the basaltic protolith metamorphosed under the amphibolite facies. It is, therefore, likely that the Prince's Town granitoids may have formed by similar processes. The Prince's Town granitoids, however, show a lower degree of REE fractionation (La_N/Yb_N = 11.93–15.30) and HREE fractionation (Yb_N = 4.88–11.53), compared to the NACG. The REE patterns with unobtrusive Eu anomalies as well as the negative Nb–Ta anomalies indicate that hornblende was the main residual phase, but with some garnet at the site of partial melting at least for Samples D9021 and D9025.

Also, the major and trace elements of some of the rocks within the Prince's Town pluton, D9021 and D9025, show some geochemical similarities to adakitic rocks, such as their high Na_2O/K_2O, $(La/Yb)_N$ and Sr/Y ratios. The petrogenesis of adakitic rocks is controversial, and different models have been proposed to account for their origin. Notably among these models are included (a) partial melting of a

TABLE 5 Sr–Nd isotopic compositions of Palaeoproterozoic rocks from the southern Ashanti volcanic belt, Ghana

Sample	Rb (ppm)	Sr (ppm)	$^{87}Rb/^{86}Sr$	$^{87}Sr/^{86}Sr$	2σ ($X10^{-6}$)	$(^{87}Sr/^{86}Sr)_{2.1}$	Sm (ppm)	Nd (ppm)	$^{147}Sm/^{144}Nd$	$^{143}Nd/^{144}Nd$	2σ ($X10^{-6}$)	ε_{Nd} (2.1 Ga)	T_{DM1} (Ga)	T_{DM2} (Ga)	$f_{Sm/Nd}$
Axim gabbroic body															
D9031 (Gabbro)	61	532	0.3319	0.711016	14	0.700971	2.46	11	0.1353	0.511726	9	−1.23	2.55	2.47	−0.312
D9035 (Gabbro)	50	815	0.1775	0.706410	12	0.701038	3.76	15.8	0.1440	0.511849	8	−1.17	2.61	2.47	−0.268
Kegyina gabbroic body															
D9039 (Gabbro)	8	520	0.0445	0.703013	11	0.701666	5.04	18.2	0.1675	0.512187	5	−0.94	2.86	2.47	−0.148
D90310 (Gabbro)	6	61	0.2846	0.710010	11	0.701394	3.88	15.7	0.1495	0.512193	8	4.07	2.00	2.03	−0.240
D90311B (Gabbro)	63	538	0.3390	0.712596	11	0.702336	0.65	2.75	0.1430	0.511919	10	0.46	2.40	2.32	−0.273
Aketakyi gabbroic body															
D9043 (Gabbro)	12	173	0.2007	0.708362	14	0.702287	1.47	4.22	0.2107	0.513099	7	5.23	5.16	2.19	0.071
Prince's Town granitoid															
D9023A (Qtz diorite)	77	380	0.5864	0.710929	10	0.693178	3.97	20.9	0.1149	0.511656	9	2.92	2.12	2.12	−0.416
D9025 (Granodiorite)	46	655	0.2032	0.707690	13	0.701540	2.76	14.9	0.1121	0.511416	8	−1.01	2.43	2.45	−0.430
D9038 (Granodiorite)	75	366	0.5934	0.717431	15	0.699468	3.95	21.6	0.1106	0.511456	7	0.16	2.33	2.35	−0.438
Ahama mafic-ultramafics															
D8301B (Pyroxenite I)	13	214	0.1757	0.706628	14	0.701309	1.66	5.93	0.1694	0.512133	7	−2.49	3.20	2.61	−0.139
D8302 (Pyroxenite I)	14	584	0.0693	0.703508	11	0.701409	1.45	5.4	0.1625	0.512135	9	−0.58	2.71	2.43	−0.174
D90211C (Pyroxenite II)	16	571	0.0810	0.703693	12	0.701240	4.61	14.9	0.1872	0.512269	9	−4.66	5.53	3.05	−0.048
D90212C (Pyroxenite II)	7	502	0.0403	0.702932	13	0.701711	3.08	9.77	0.1907	0.512266	7	−5.68	-	-	−0.030
Aketakyi UMC															
D90410 (Metaperidotite)	1	22	0.1315	0.704456	12	0.700477	0.70	2.17	0.1952	0.51284	8	4.38	1.63	2.01	−0.008
D90411B (Metaperidotite)	<1	10	-	0.705412	14	-	0.40	1.28	0.1891	0.512784	8	4.93	1.57	1.96	−0.039
D90413 (Metaperidotite)	<1	10	-	0.705089	14	-	0.11	0.32	0.2080	0.512982	14	3.69	0.63	2.01	0.057

Note. ε_{Nd} values calculated at 2.1 Ga, relative to the present-day chondritic values of $^{143}Nd/^{144}Nd = 0.512638$ and $^{147}Sm/^{144}Nd = 0.1967$ $f_{Sm/Nd} = [(^{147}Sm/^{144}NdSample)/(^{147}Sm/^{144}Nd_{CHUR})]-1$. T_{DM1} and T_{DM2} are single-stage and two-stage Nd model ages; T_{DM1} is computed according to the depleted mantle model of Ben Othman, Polvé, and Allègre (1984) and T_{DM2} following the approach of Keto and Jacobsen (1987).

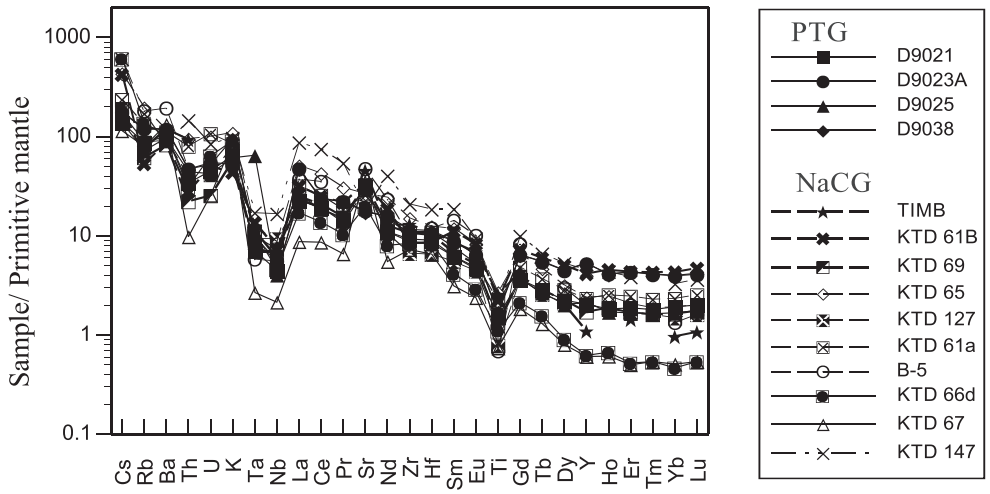

FIGURE 9 Primitive-mantle-normalized multi-element patterns of Prince's Town granitoids (PTG) compared with sodic calc-alkaline Birimian granitoids (NaCG) reported from central Cote d'Ivoire (Doumbia et al., 1998). Normalization values are from Sun and McDonough (1989)

TABLE 6 Composition of the Prince's Town granItoids compared with the average compositions of adakites, TTGs, sanukitoids, closepet-type and experimental melts

	D9021	D9023A	D9025	D9038	LSA[a]	HAS[a]	TTG1[a] >3.5 Ga	TTG2[a] 3–3.5 Ga	TTG3[a] <3.5 Ga	Sanukitoids[a] <62%	Closepet[a] <62%	Experimental melts[a]
In wt.%												
SiO_2	66.66	62.96	70.49	68.30	56.25	64.8	69.59	69.65	68.36	58.76	56.39	68.94
TiO_2	0.34	0.36	0.27	0.38	1.49	0.56	0.39	0.36	0.38	0.74	1.2	0.78
Al_2O_3	16.05	16.33	15.72	14.50	15.69	16.64	15.29	15.35	15.52	15.8	15.79	17.7
Fe_2O_3	3.91	5.75	3.10	4.23	6.47	4.75	3.26	3.07	3.27	5.87	7.34	2.42
MnO	0.08	0.11	0.06	0.08	0.09	0.08	0.04	0.06	0.05	0.09	0.13	0.05
MgO	2.05	2.72	1.53	2.14	5.15	2.18	1	1.07	1.36	3.9	3.38	0.84
CaO	3.90	5.63	3.30	3.48	7.69	4.63	3.03	2.96	3.23	5.57	5.45	2.06
Na_2O	4.74	3.74	4.75	3.95	4.11	4.19	4.6	4.64	4.7	4.42	3.94	4.92
K_2O	1.98	1.64	1.87	2.95	2.37	1.97	2.04	1.74	2	2.78	3.17	2.53
P_2O_5	0.13	0.12	0.10	0.11	0.66	0.2	0.13	0.14	0.15	0.39	0.72	
In ppm												
V	73	74	49	76	184	95	39	43	52	95	129	25
Cr	200	200	160	170	157	41	34	21	50	128	50	
Co	13	13	27	13								
Ni	90	80	80	70	103	20	12	15	21	72	38	16
Cu	40	20	20	40								
Zn	60	50	50	50								
Ga	20	16	20	16								
Ge	1	1.1	1	1.2								
Rb	55	77	46	75	19	52	79	59	67	65	93	98
Sr	667	380	655	366	2,051	565	360	429	541	1,170	978	333
Y	9.3	23.9	9.7	24.3	13	10	12	14	11	18	37	11.9
Zr	104	118	98	130	188	108	166	155	154	184	323	196

(Continues)

TABLE 6 (Continued)

	D9021	D9023A	D9025	D9038	LSA[a]	HAS[a]	TTG1[a] >3.5 Ga	TTG2[a] 3–3.5 Ga	TTG3[a] <3.5 Ga	Sanukitoids[a] <62%	Closepet[a] <62%	Experimental melts[a]
Nb	3.2	4	2.9	4	11	6	8	6	7	10	18	11.4
Sn	<1	1	<1	1								
Cs	1.1	1.4	1.1	1.4								
Ba	712	837	681	845	1,087	721	449	523	847	1,543	1,441	651
La	15.8	32.7	17.7	32.7	41.1	19.2	35.3	31.4	30.8	59.9	90.9	28.65
Ce	33.8	42.4	33.2	41.5	89.8	37.7	61.7	55.1	58.5	126	188	53.56
Pr	4	6.18	4.18	6.16								
Nd	14.9	20.9	14.9	21.6	47.1	18.2	25.8	19.6	23.2	54.8	84.9	25.05
Sm	2.76	3.97	2.76	3.95	7.8	3.4	4.2	3.3	3.5	9.8	14.5	
Eu	0.812	1.09	0.775	1.08	2	0.9	1	0.8	0.9	2.3	3.2	1.23
Gd	2.16	3.85	2.16	3.82	4.8	2.8	3.2	2.4	2.3	6	9.2	
Tb	0.31	0.59	0.29	0.6								
Dy	1.65	3.31	1.5	3.33	2.8	1.9	1.8	1.9	1.6	3.2	5.6	2.35
Ho	0.3	0.68	0.28	0.67								
Er	0.9	2.07	0.8	2.08	1.21	0.96	0.77	0.77	0.75	1.41	2.68	1.21
Tm	0.134	0.303	0.121	0.306								
Yb	0.95	1.95	0.83	1.96	0.93	0.88	0.78	0.63	0.63	1.32	2.05	0.94
Lu	0.148	0.303	0.13	0.31	0.08	0.17	0.2	0.13	0.12	0.26	0.34	
Hf	2.8	3.3	2.6	3.5								
Ta	0.29	0.35	2.66	0.4								
W	<0.5	0.7	80.1	2.1								
Tl	0.36	0.36	0.24	0.42								
Pb	12	9	9	11								
Bi	0.6	0.4	0.5	0.4								
Th	2.9	4.01	3.77	4.03								
U	0.95	1.15	0.89	1.1								

[a]Data from Martin et al. (2005).

subducting oceanic slab (e.g., Defant & Drummond, 1990; Martin, Smithies, Rapp, Moyen, & Champion, 2005), (b) crustal assimilation and fractional crystallization (AFC) processes from parental basaltic magmas (Castillo et al., 1999), (c) partial melting of a stalled (or dead) slab in the mantle (e.g., Qu, Hou, & Li, 2004), (d) partial melting of delaminated lower crust (e.g., Kay & Mahlburg Kay, 1993; Wang et al., 2006), and (e) partial melting of mafic rocks in the lower part of thickened crust (Atherton & Petford, 1993; Petford, Atherton, & Halliday, 1996). On the basis of an extensive adakite geochemical database, Martin et al. (2005) have grouped adakites into two groups: high-SiO_2 (HSA) and low-SiO_2 (LSA) adakites. High-SiO_2 (HSA) have SiO_2 (>60 wt.%), MgO (0.5 to 4 wt.%), CaO + Na_2O (<11 wt.%), and Sr (<1,100 pm), compared to LSA with SiO_2 (<60 wt.%), MgO (4 to 9 wt.%), CaO + Na_2O (>10 wt.%) and Sr (>1,000 ppm).

The HSA are considered to be product of subducted basaltic slab melts that have reacted with peridotite during its ascent through mantle wedge, whereas LSA are believed to have been generated by melting of a peridotitic mantle wedge whose composition has been modified by reaction with felsic slab melts (Martin et al., 2005). Samples D9021 and D9025 are similar to HSA (Table 6; Figure 10) and may have been generated by similar processes.

Mauer (1990) indicated that the belt-type granitoids and tholeiitic basalts of Ghana are genetically closely related and that the granitoids were derived from partial melting of the tholeiitic basalts. This claim is corroborated by Hirdes et al. (1992), who also indicated from their isotopic data that the belt volcanic rocks and belt granitoids are coeval and comagmatic, and were formed at different stages of the same igneous event. The major element data also suggest that the Prince's Town plutonics were mostly likely derived from the metavolcanics.

The analysed granitoids are characterized by negative and positive ε_{Nd} (2.1 Ga) values ranging from −1.01 to +2.92 and T_{DM2} of 2.12–2.45 Ga. The relatively high positive initial ε_{Nd} of +2.92 and Protereozioc Nd model age of 2.17 Ga obtained for a quartz diorite (D9023A) suggest that it was juvenile at its time of formation. For

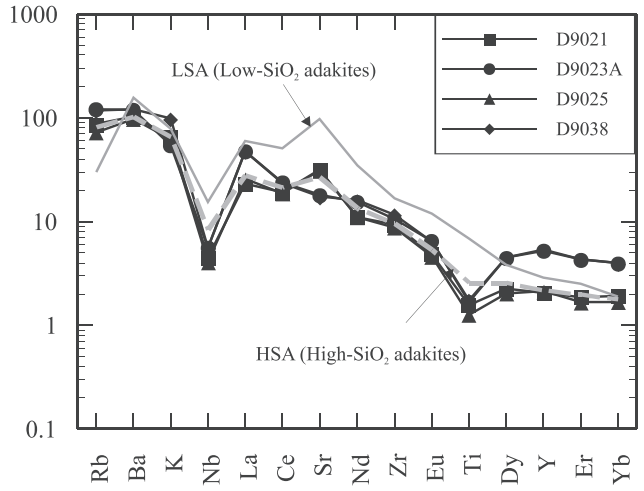

FIGURE 10 Compositions of the Prince's Town granitoids compared with those of the average adakites (after Martin et al., 2005)

the other granodioritic samples (D9025 and D9038), the ε_{Nd} (2.1 Ga) values of −1.01 and +0.16 with Nd model ages of 2.45 and 2.35 Ga suggest partly enriched mantle sources. The granitoids, however, demonstrate primitive initial $^{87}Sr/^{86}Sr$ ratios of ~0.700. Therefore, the isotopic signatures of the Prince's Town granitoids are indicative of juvenile crust which may have been contaminated by some amount of an older crustal component. A slightly crustal contamination of the granitoids is also demonstrated by the inverse correlation between ε_{Nd} (2.1) and SiO_2 (Figure 11).

5.2.2 | Mafic and ultramafic rocks

Fractional crystallization and crustal contamination

The Ahama pyroxenites, Aketakyi, Axim, and Kegyina gabbroic rocks exhibit chemical characteristics different from the Aketakyi UMC in MgO variation diagrams (Figure 7). Loh and Hirdes (1999) performed XRF analysis on these rocks, except the Kegyina gabbros, and their chemical data are included in the MgO variation plots. The Aketakyi gabbroic rocks display a common evolutionary trend in MgO variation diagrams (Figure 7). The Al_2O_3 and CaO contents are negatively correlated with MgO, which suggest fractionation of pyroxene. The K_2O and Na_2O display a negative correlation with MgO, suggesting fractionation of hornblende. The role played by plagioclase is envisaged in the evolution of these magmas, as well as other gabbroic bodies, based on their variable Eu anomalies (Figure 4b). In the Axim and Kegyina gabbros as well as the Ahama pyroxenites, Al_2O_3 and CaO are again correlated negatively with MgO, whereas the Cr and Ni correlate positively with MgO. These trends suggest fractionation of olivine and pyroxene (Figure 7). The rocks also show similar evidence of fractionation of hornblende as the Aketakyi gabbroic rocks. A well-defined negative correlation between TiO_2 and MgO suggests fractionation of Fe–Ti oxides. Although the Ahama pyroxenites, Aketakyi, Axim, and Kegyina gabbroic rocks demonstrate some similarities in the MgO variation diagrams (Figure 7), some chemical variations, including REE patterns (Figure 4b,c), exist among these individual bodies, which suggest that they cannot be related in a single line of descent from a single parental magma via fractional crystallization. The variation in the Nd isotopic composition of these magmatic rocks (Table 5) also precludes them from being part of a single magmatic system. Variations in the Sr–Nd isotopic composition of magmatic rocks are commonly explained by either crustal contamination or heterogeneous mantle sources.

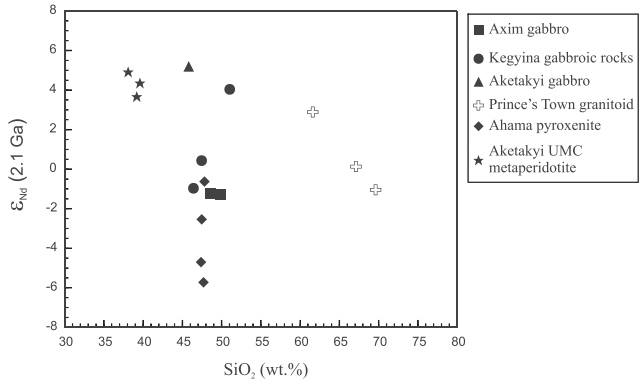

FIGURE 11 Plots of ε_{Nd} (2.1 Ga) versus SiO_2, TiO_2, and P_2O_5 (wt.%) for the Palaeoproterozoic rocks from the Ashanti volcanic belt

Crustal contamination in the magmatic rocks was visualized in the plot of ε_{Nd} (T) versus SiO_2 (Figure 11). The lack of systematic trend of decreasing ε_{Nd} (T) values with increasing SiO_2, as would be expected in rocks affected by crustal contamination, suggests that crustal contamination was minimal in the magmas of these mafic and ultramafic bodies. The mafic and ultramafic rocks display negative Nb and Ta anomalies relative to LILE and LREE in the primitive-mantle-normalized, trace element diagrams (Figure 5b,c). Crustal contamination could also produce such anomalies but would also result in positive Zr–Hf anomalies due to enrichment of these elements in crustal materials (Zhao & Zhou, 2007). Taylor and McLennan (1985) have also indicated that upper crustal rocks are typically enriched in U, Zr and Hf elements, and depleted in Nb, Ta, and Ti. Thus, the negative U, Th, Zr, and Hf anomalies in the rocks (Figure 5b,c) cannot be explained by upper crustal contamination. Therefore, the negative Zr–Hf anomalies in the rocks suggest that only little or no crustal contamination occurred in them. Crustal components are also rich in Th and Pb. Thus, low and constant Th and Pb, low Th/Yb, and high Nb/Th ratios in the rocks are also inconsistent with crustal contamination (Figure 12). However, compared to the gabbroic rocks, the Axim gabbros have slightly higher Th and Pb contents, and higher Th/Yb and ratios, suggesting some small degree of crustal contamination might have occurred (Table 2; Figure 12a,c).

Nature of the mantle source region

High Nb and Ta values in magmatic rocks have been interpreted to indicate oceanic island basalt (OIB) component in those rocks (e.g., Edwards et al., 1994; Zou, Zindler, Xu, & Qu, 2000). The Axim, Kegyina, and Aketakyi rocks show depletion in Nb and Ta. The Ahama pyroxenitic rocks also display negative Nb–Ta anomalies (Figure 5). Negative Nb–Ta anomalies may also be caused by crustal contamination. However, the negative Zr–Hf anomalies observed in the rocks are inconsistent with crustal contamination, as crustal materials are

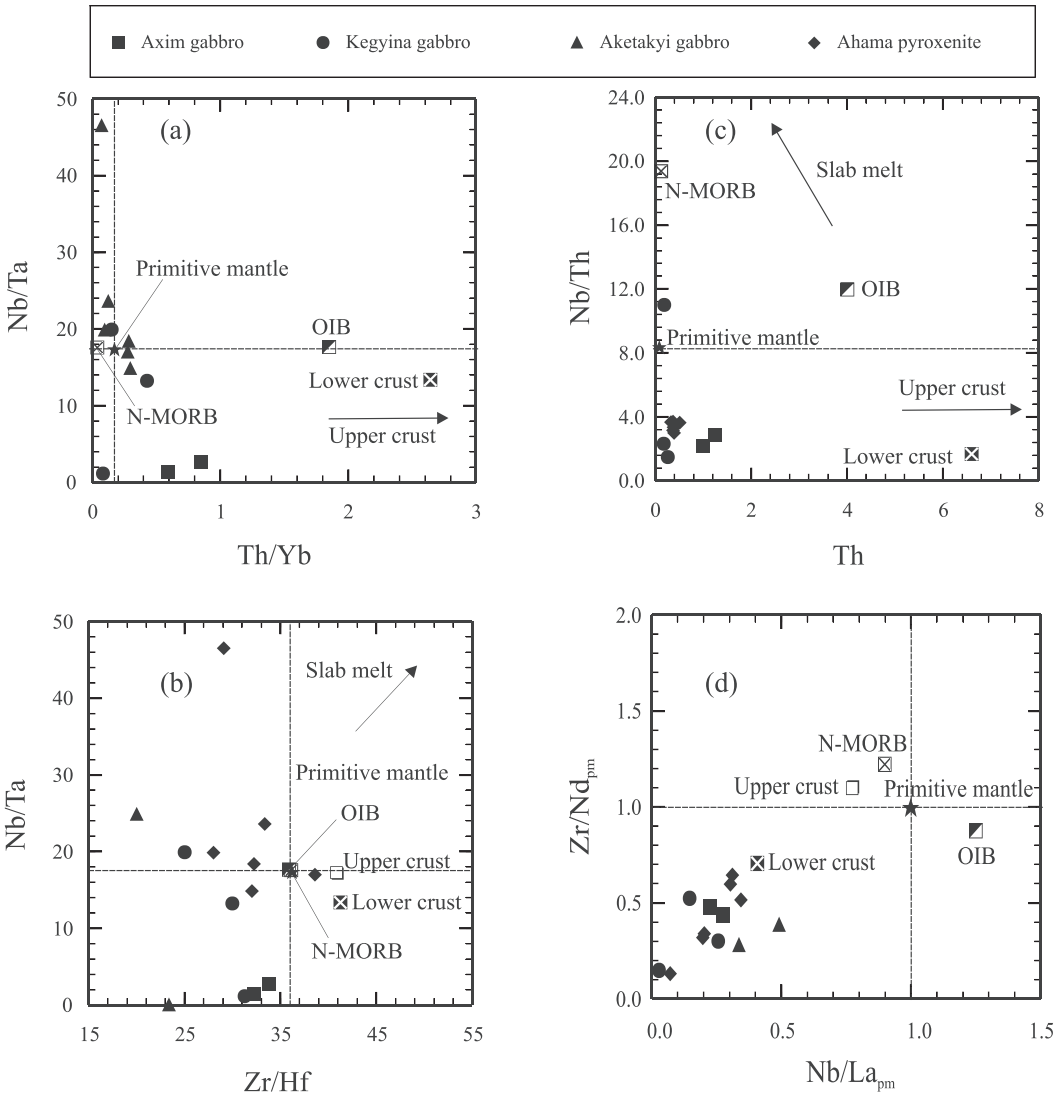

FIGURE 12 Plots of (a) Nb/Ta vs. Th/Yb, (b) Nb/Ta vs. Zr/Hf, (c) Nb/Th vs. Th, and (d) Zr/Nd_{pm} vs. Nb/La_{pm} for the gabbroic and pyroxenitic rocks from the southern Ashanti greenstone belt. Values of N-MORB, OIB, and primitive mantle are from Sun and McDonough (1989). Values for the upper and lower crust are from Wedepohl (1995)

enriched in elements such as Th, Zr, Hf, and so on (Figure 5b,c). Negative Zr–Hf anomalies are not common among intraplate basalts (Zhou, Kennedy, Sun, Malpas, & Lesher, 2002). Thus, the negative Nb and Ta and Zr–Hf anomalies indicate the lack of an OIB component in their source region. Rather, the gabbroic and pyroxenitic rocks may have been derived from lithospheric mantle sources.

Pearce and Peate (1995) have indicated that the budget of moderately incompatible elements (HREE, HFSE, and Ti) is mainly controlled by partial melting processes, and such elements may be used to estimate the degree of the source depletion (Woodhead, Eggins, & Gamble, 1993). It has been indicated that the HFSE may be used to constrain the nature of the mantle sources which may have been depleted by previous melt extraction in back-arc basins (Elliott, Plank, Zindler, White, & Bourdon, 1997; Woodhead et al., 1993) or in arc settings (Grove, Parman, Bowring, Price, & Baker, 2002). Experimental studies have shown that Nb–Ta and Zr–Hf have considerably different partition coefficients in the system clinopyroxene/anhydrous silicate melt (Hart & Dune, 1993; Johnson, 1998), where Zr is mostly more incompatible than Hf by a factor of 1.5–2, and the D_{Nb}/D_{Ta} ratio is less than 1. Consequently, Nb/Ta and Zr/Hf could be significantly fractionated and would be positively correlated during partial melting of the upper mantle. Plank and White (1995) have indicated that mantle wedge-derived arc basalts may inherit such ratios, reflecting variable degrees of mantle depletion produced prior to episodes of melt generation. In view of this, very low HFSE contents and small Nb/Ta ratios in arc volcanic rocks are believed to reflect previous melt extraction from the mantle wedge (Woodhead et al., 1993). Woodhead et al. (1993) and Pearce and Peate (1995) have indicated the process involved in the melt extraction would also lead to positive correlations of sub-chondritic Nb/Ta ratios with La/Yb, Th/Yb, Zr/Yb, Zr/Ti, Ti/V, and Y/Sc ratios, which would decrease with increasing depletion of the mantle wedge. However, the pyroxenitic and gabbroic rocks largely do not exhibit such consistency in the elemental correlations (Figure 12b,d). It appears, therefore, that the mantle source region of

the rocks was a normal lithospheric mantle wedge, which had not been depleted by previous melt extraction.

Gabbros D9042 and D9043 from the Aketakyi gabbroic body reveal LREE-depletion as in MORB yet an overabundance of fluid-soluble elements that indicate a slab-derived component (Figures 4b and 5b). The high initial ε_{Nd} value of +5.23 in the D9043 indicates depleted upper mantle sources. Its Nd model age of 2.15 Ga suggests a juvenile character. The initial $^{87}Sr/^{86}Sr$ ratio of 0.702287 obtained for D9043 suggest a small degree of crustal contamination of the mantle melt. The LREE-depleted gabbroic samples probably originated at a back-arc-basin spreading centre where LREE depleted rocks with enrichment of fluid mobile elements are ubiquitous (e.g., Bach, Hegner, & Erzinger, 1998; Jenner, Cawood, Rautenschlein, & White, 1987). The analysed Axim gabbros show consistent negative initial ε_{Nd} values (−1.23 and −1.17) but low initial $^{87}Sr/^{86}Sr$ ratios (0.700971 and 0.701038). The Nb depletion relative to the LREEs, negative Nb–Ta and Zr–Hf anomalies (Figures 4b and 5b), relatively high LILE/HREE (or LILE/HFSE) ratios as well as their low initial ε_{Nd} values could be interpreted as the signatures of the addition of subduction-related fluids into a depleted mantle source (Kepezhinskas et al., 1997). The high Nd model ages (T_{DM2}) of 2.54 and 2.55 Ga obtained for the Axim gabbros suggest an input of a pre-Birimian crustal component in their formation, probably through subduction. The Axim gabbros most likely originated from a subduction-related lithospheric mantle. The Kegyina gabbroic body demonstrates a wide range of initial ε_{Nd} values (−0.94, 0.46, and 4.07) which indicates partly enriched mantle and depleted mantle sources. Sample D90310 with high initial ε_{Nd} value (+4.07) show similar characteristics as the Aketakyi gabbro D9043 but shows LREE-enrichment. D90310 demonstrates a Proterozoic Nd model age (2.08 Ga), suggesting a juvenile character. The ε_{Nd} (2.1) values of −0.94 and +0.46 obtained for the other Kegyina rocks, D9039 and D90311B, with respective Nd model ages of +2.57 and +2.39 are indicative of some contamination of their mantle belts by older crustal materials. Like the Axim gabbros, they could have also originated from a subduction-related lithospheric mantle. The analysed Ahama pyroxenitic rocks have initial $^{87}Sr/^{86}Sr$ ratios of 0.701211–0.701711, which indicate minimum crustal contamination of the mantle melt. The ε_{Nd} (2.1) values of these samples are −0.58, −2.49, −4.66, and −5.68, indicative of partly enriched to enriched mantle products. The pyroxenitic rocks display Nb depletion relative to the LREEs, negative Nb–Ta and Zr–Hf anomalies (Figure 5 c), relatively high LILE/HREE (or LILE/HFSE) ratios, and these features combined with their low initial ε_{Nd} values could point to subduction-related lithospheric mantle sources. Their high negative ε_{Nd} (2.1) values and Nd model ages of 2.52 and 2.75 Ga are possibly indicative of a greater subduction input of an older crustal material.

Source modification by subduction components

The mantle wedge above a subduction zone may be modified by components from the down-going slab by processes such as (a) fluxing of fluids derived from dehydration of altered oceanic crust (Hawkesworth, Turner, McDermott, Peate, & van Calsteren, 1997) or subducted sediments (e.g., Class, Miller, Goldstein, & Langmuir, 2000) and (b) addition of melts of subducted sediment (e.g., Münker, 2000) or melts of the MORB portion of the slab (Peacock, Rushmer, & Thompson, 1994). As demonstrated earlier, the trace element geochemical signatures of the gabbroic and pyroxenitic rocks suggest that they may have been derived from a metasomatized lithospheric mantle source above a subduction zone.

The abundance of highly incompatible elements in magma is controlled by fluid influx (Stolper & Newman, 1994). Rare earth elements and HFSE (e.g., Th, Zr, Hf, Nb, and Ta) are relatively immobile in aqueous fluids (Keppler, 1996; Turner et al., 1997), compared with LILE. Therefore, the enrichment of REE and HFSE in a mantle wedge is attributed to inputs of slab melts rather than aqueous fluids (Elliott et al., 1997; Plank & Langmuir, 1992). Mantle sources modified by slab melts may have lower Th/Zr, Rb/Y (Kepezhinskas et al., 1997), Ba/Nb and Ba/Th ratios (Hawkesworth et al., 1997) than those modified by fluids. The chemical compositions of the gabbroic and pyroxenitic rocks suggest that their mantle sources experienced largely fluid and some melt metasomatism above a subduction zone.

The Ahama Group I pyroxenites show Th–U and Nb–Ta troughs, positive Sr anomalies, and minor negative Zr–Hf and Ti anomalies, whereas the Group II pyroxenites exhibit negative Th anomalies, pronounced negative Nb, Zr–Hf and Ti anomalies, and spikes in Sr (Figure 5c). The Th/U ratios of the Ahama Group I pyroxenites vary from 2.24 to 2.91 and are relatively higher than those of the Group II rocks (0.79–1.96); both types have Th/U ratios less than those of OIB (3.5–3.8) and enriched mantle (EMI) which range from 4.5 to 4.9 (Weaver, 1990). It is noted that Zr/Nb ratios in mafic rocks range from about 40 in mid-ocean ridge basalt (MORB) to 10 in E-type MORB and to <10 in OIB and rift-related lavas (Pearce & Norry, 1979). The Zr/Nb ratios of the pyroxenites vary from 21 and 27, falling between OIB and MORB, but comparable with the Zr/Nb ratios of the associated LREE-enriched basalts and andesites from the southern Ashanti volcanic belt (Dampare, Shibata, Asiedu, Osae, & Banoeng-Yakubo, 2008). Loh and Hirdes (1999) obtained Zr/Nb ratios of 5–34 for the pyroxenites, similar to this study. They also have high Ba/Nb (95–207), Ba/Zr (4–9), Ba/Th (308–588), and U/Th ratios (0.3–0.7) relative to the primitive mantle. Loh and Hirdes (1999) also obtained high Ba/Nb (39–305), Ba/Zr (8–9), Ba/Th (194–305), and U/Th (1) ratios for the pyroxenites. Such high elemental ratios in the pyroxenites, which are also higher than those of the average upper crust, suggest that they were more likely derived from a mantle source strongly modified by hydrous fluids. The Axim gabbroic rocks also exhibit high ratios of Ba/Nb (166–390), Ba/Zr (10–19), Ba/Th (485–866), and U/Th ratios (0.4) relative to the primitive mantle. These observations are consistent with the previous work by Loh and Hirdes (1999), who obtained Ba/Nb, Ba/Zr, Ba/Th, and U/Th ratios of 421–565, 7–9, 22–565, and 0.1–1, respectively, for the Axim gabbroic rocks. The Kegyina gabbroic rocks have higher ratios of Ba/Nb (42–473), Ba/Zr (2–16), Ba/Th (146–1,112), and U/Th ratios (0.3–1.27) relative to the primitive mantle, also indicating that their mantles were strongly modified by hydrous fluid. The Aketakyi gabbroic rocks have higher ratios of Ba/Nb (72–90) and Ba/Zr (4) but retain very low Th concentrations. Loh and Hirdes (1999) obtained Ba/Nb (47–93), Ba/Zr (1–7), Ba/Th (47–93), and

U/Th ratios of 47–93, 1–7, 47–93, and 1, respectively. Thus, the mantle source of the Aketakyi gabbroic rocks may not have been modified significantly by slab-derived fluids.

It can be inferred from the chemical and isotopic composition of the rocks that the Ahama pyroxenites were extracted from a more fluid-metasomatized mantle different from that of Axim, Kegyina, and Aketakyi gabbroic rocks, with the mantle source of the Aketakyi gabbros being the least metasomatized. These mafic and ultramafic rocks, which are genetically unrelated and have different emplacement records, were later juxtaposed. The Aketakyi gabbros are associated with the LREE-depleted, back-arc basin basalts, the sheet-dyke complex, and the Aketakyi ultramafic rocks in the study area, and they could be part of an obducted piece of a back-arc basin. The Prince's Town pluton intrudes the western flank of the Aketakyi ultramafic complex (Attoh et al., 2006), and the Aketakyi gabbro is inferred to have been emplaced earlier than the Prince's Town pluton. In the field, the Axim gabbroic body occurs to the west of the Prince's Town pluton and is associated with argillite and andesitic lavas in the transition zone between the Kumasi basin and the Ashanti belt. The Axim body is believed to have been emplaced later than the granitoids. The Ahama ultramafic body is located to north of the Axim volcanic belt (Figure 2) is associated with the LREE-enriched volcanic arc basalts and andesites (Dampare, Shibata, Asiedu, Osae, & Banoeng-Yakubo, 2008). The volcanic rocks are also intruded by the Prince's Town pluton, but the relationship between the Ahama ultramafic body and the Prince's Town pluton is uncertain. The Kegyina mafic body occurs at the margin of the Prince's Town pluton and could be coeval with the latter. The Aketakyi gabbro is inferred to have been emplaced earlier than the Prince's Town pluton, as the latter intrudes the western flank of the Aketakyi ultramafic complex, of which the Aketakyi gabbro is considered to be part.

Aketakyi ultramafic complex

Ultramafic–mafic rocks have diverse origins and could represent one of the following: (a) fertile upper mantle, (b) residual upper mantle, and (c) ultramafic cumulate in large magma chambers at the base of the crust. Ultramafic–mafic rocks can occur as complete or incomplete ophiolitic complexes as well as rootless bodies tectonically emplaced into lower and upper crustal rocks.

The chemical compositions of the analysed rocks from the Aketakyi UMC have provided some useful petrogenetic information about the rocks. Petrographically, the rocks from the Aketakyi UMC appear to be crystal cumulates, and this is confirmed by the geochemical data (Table 4). Trace elements are depleted in the rocks as a result of the cumulate effect. Crystal fractionation is suggested by MgO variation diagrams (Figure 7), which include the chemical data of the present study and that of Loh & Hirdes (1999). The compatible trace elements Ni, Co, and Cr are positively correlated with MgO. Nickel is mainly controlled by fractionation and accumulation of olivine, unless sulphide is present in the magma. Cobalt is also controlled mainly by fractionation and accumulation of olivine. Chromium is controlled by fractionation of chromite and diopside, and V is controlled by fractionation and accumulation of magnetite. The Ga and V contents of the rocks show an inverse correlation with MgO, reflecting their incompatible behaviour. The abundances of Al_2O_3, Na_2O, CaO, and SiO_2 are inversely correlated with MgO (Figure 7). The negative correlation of SiO_2 and Al_2O_3 with MgO indicates fractionation of silica-poor, magnesia-rich minerals such as orthopyroxene and olivine. The observed trends in variation diagrams suggest fractional crystallization of olivine and pyroxene. The pyroxenitic-gabbroic varieties have higher Sr contents than the peridotites, signifying the importance of plagioclase in their formation.

The nature of the parental magma of the ultramafics has been investigated following the method of Roeder and Elmslie (1970). The olivine composition is used to estimate the MgO/FeO value of the primary magma using Mg–Fe distribution coefficient (K_d = $[(FeO/MgO)_{ol}/(FeO/MgO)_{magma}]_{molar}$ = 0.3 ± 0.03). Although K_d is relatively insensitive to temperature, pressure, and liquid composition (Roeder & Elmslie, 1970), the cumulate olivine can be less magnesium-rich than that initially formed because of re-equilibration with the residual magma. Hence, the calculated MgO/(MgO + FeO) value might be lower than that of the parent magma. Therefore, it is better to select the most magnesian olivine in order to constrain the MgO and FeO values.

Some information on olivine compositions for the Aketakyi UMC has been provided by Attoh et al. (2006), and combining their results with those newly obtained in this study, the most magnesian olivine in this complex is Fo_{85}. Using the distribution coefficient of 0.3, Fo_{85} corresponds to a Mg# (molar ratio of MgO/(MgO + FeO)) of 0.65 in the liquid. Therefore, it can be concluded that the parent magma of the Aketakyi UMC was high in magnesium, although the precise concentrations of SiO_2, MgO, and FeO could not be obtained using this method. Thus, the ultramafic complex probably originated from a mafic magma in the greenstone belt of which the tholeiitic basalt is a possible candidate. The analysed Aketakyi meta-peridotites have Nd model ages (1.99–2.04 Ga), which suggest that they were juvenile at their time of formation. Their ε_{Nd} (2.1 Ga) values (+3.69 to +4.93) suggest they derived from depleted mantle magmas.

Brown amphibole in the Aketakyi UMC shows postcumulus textural characteristics (i.e., postcumulus phase enclosing olivine, pyroxene, and serpentinized olivine grains). The occurrence of primary magmatic amphibole suggests the presence of relatively high water contents in the parental magma. Thus, hydrous partial melting of a mantle source which had previously been metasomatized is envisaged.

5.3 | Tectonic setting considerations

5.3.1 | Southern Ashanti volcanic belt

Several schemes exist for assigning granitoids to various tectonic environments based on their geochemistry (e.g., Batchelor & Bowden, 1985; Maniar & Piccoli, 1989; Pearce, Harris, & Tindle, 1984). In this study, the trace element characteristics of the Prince's Town granitoids have been compared with a volcanic arc granite reference sample from Chile and a within-plate granite reference sample from Oslo (Pearce et al., 1984). The trace elements of the granitoids show an overall

negative slope from the LILE to the HFSE and depletion of Nb and Ta, similar to those of granitoids emplaced in a modern-day active continental margin context, such as depicted by the reference pattern of volcanic arc granite (VAG) from Chile (Figure 13). Enrichment in LILE and depletion in Nb and Ta usually characterize active margin-related magmas, whereas the development in a within-plate context would result in enrichment in Nb and Ta such as observed in the within-plate granitoid from Oslo (Figure 13). The observed tectonic setting of the Prince's Town pluton is consistent with the previous studies carried out on the granitoids from the southern Ashanti belt (Dampare et al., 2005; Loh & Hirdes, 1999) and other Birimian volcanic belts of Ghana.

The LILE and LREE enrichment and HFSE depletion in the Ahama pyroxenites and, the Axim, Kegyina and Aketakyi gabbroic rocks indicate involvement of subduction-related components in their source region (Figure 5). Their geochemical signatures resemble those of the associated metavolcanic rocks, which formed in an intra-oceanic island arc–back-arc environment (Dampare, Shibata, Asiedu, Okano, et al., 2008), and those of island arc intrusions (e.g., Zhou et al., 2002), suggesting a subduction zone setting. Thus, these mafic and ultramafic intrusions were derived from arc-related magmatism during the Palaeoproterozoic.

Ultramafic rocks may be subdivided according to their geotectonic setting into the subcontinental and suboceanic mantle, including mantle underneath oceanic ridges, oceanic islands, oceanic plateaus, island arcs, fore- and back-arc regions, and so on (e.g., Bonatti & Michael, 1989). Also, the upper mantle can be pervasively metasomatized, or affected by melt–rock, melt–fluid, and rock–fluid interactions. The Aketakyi ultramafic complex has previously been suggested to represent a fragment of a Palaeoproterozoic ophiolitic complex emplaced in a supra-subduction zone (SSZ) tectonic setting (Attoh et al., 2006). The inferred tectonic setting of the complex is further supported by

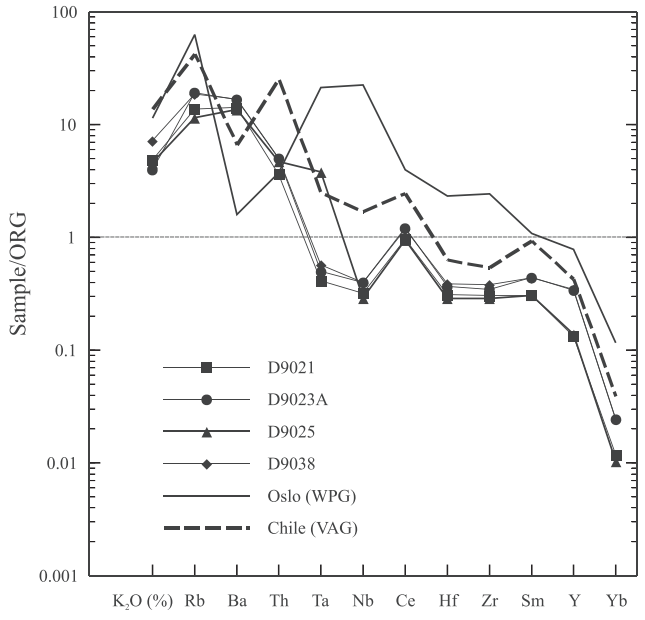

FIGURE 13 Ocean ridge granite (ORG)-normalized spider diagram of the Prince's Town granitoid. The ORG normalization values and data for volcanic arc and within-plate granites are from Pearce et al. (1984)

the following lines of evidence: (a) some of the rocks display LREE-depleted MORB-like patterns; such patterns are not only restricted to MORB but could also be observed in magmas at back-arc basin; (b) some of the rocks show slight depletion in Nb, Ta, Zr–Hf, and Ti (i.e., mild subduction-zone signature; Figure 5c). Almost all the rocks demonstrate strong enrichment in Cs; however, Cs enrichment could also result from serpentinization. Although these arc-/subduction-related features are not observed in all the rocks analysed, it is difficult to envisage how they could have formed in different tectonic settings; (c) the basaltic rocks associated with the ultramafic complex show geochemical signatures characteristic of back-arc basin basalts; and (d) the Prince's Town granitoids, which intruded into the western flank of the ultramafic complex, are island arc-related granitoids. Thus, the Aketakyi UMC formed in a supra-subduction zone environment.

The geotectonic environment in which the plutonic rocks were formed or emplaced has also been investigated in the plot of $f_{Sm/Nd}$ versus ε_{Nd} (2.1 Ga). Most of the rocks fall in and close to the field of the Proterozoic arc crust (Figure 14; Roddaz et al., 2007 and the references therein). Indeed, their ε_{Nd} (2.1 Ga) values overlap the fields of Palaeoproterozoic arc crust and MORB. The Aketakyi UMC metaperidotites plot in the arc field, thereby demonstrating their affinity for a supra-subduction environment.

The southern Ashanti volcanic belt consists of serpentinized peridotites, pyroxenites, gabbros, granitoids, and metavolcanic rocks. However, the real relationship between the rocks is obscured because of lack of definite isochron ages and poor outcrop exposure. The supra-subduction zone setting proposed for these rocks is mainly based on geochemical, isotopic, and field observations outlined here: (a) The association of pillow basalt and gabbros, pronounced development of andesitic flows and pyroclastic rocks as well as occurrence of cherty rocks in the belt suggest an intra-oceanic depositional environment. (b) The high initial ε_{Nd} (2.1) isotopic values (e.g., +4.38 to +5.23) of some of the plutonic rocks indicate a long-term LREE-depleted mantle source(s), similar to the source of modern N-MORB (see Hofmann, 2003). High initial ε_{Nd} (2.1) isotopic values of +3.89 to +7.21 were also obtained for tholeiitic basalts in the volcanic belt (Dampare, Shibata, Asiedu, Osae, & Banoeng-Yakubo, 2008). However, some of the rocks have Nb-depleted, relative to Th and La, trace element patterns (Dampare, Shibata, Asiedu, Osae, & Banoeng-Yakubo, 2008; this study), consistent with a subduction zone geodynamic setting. (c) Large variations in the initial ε_{Nd} values may reflect either mantle source heterogeneity or crustal contamination. As discussed in the previous sections, contamination by continental crust during magma ascent, rather than contamination of their source regions by subducted crustal material, may be minimal. (d) Adakitic (this study) and boninitic (Dampare, Shibata, Asiedu, Osae, & Banoeng-Yakubo, 2008) signatures observed in some of the rocks also support subduction-zone environment. In this context, the generated supra-subduction zone (SSZ) oceanic crust in the back-arc basin consists of the Aketakyi ultramafic-mafic complex, Aketakyi gabbro, and BABB-type basalts (massive and pillowed lavas). This probably represents an upper mantle transition and crustal section of a back-arc basin ophiolitic complex. The arc magmatism in the study area is

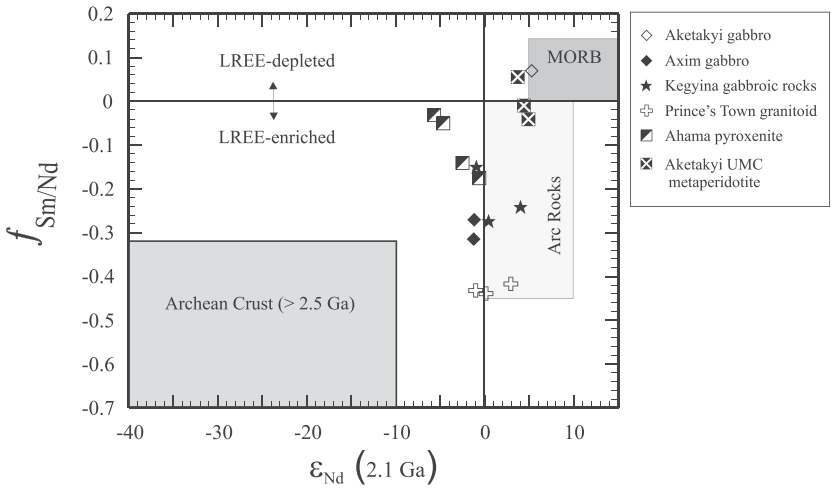

FIGURE 14 Plot of ε_{Nd} (2.1 Ga) versus fractionation parameter ($f_{Sm/Nd}$). Fields of old (Archaean) continental crust, MORB, and the arc rocks are from Roddaz et al. (2007) and the references therein

characterized by island arc calc-alkaline series volcanics (Dampare et al., 2008), mafic (Axim and Kegyina gabbroic rocks), and ultramafic (Ahama pyroxenitic rocks) rocks as well as the Prince's Town granitoid. These supra-subduction rocks were accreted to the continental margin. Thus, the volcanic and plutonic rocks of the southern Ashanti greenstone belt consist of an association of island arc and back-arc sequences that have been amalgamated during subduction–accretion and collisional obduction.

5.3.2 | Ashanti belt and the WAC

As was mentioned in the earlier section, the geotectonic setting of the Palaeoproterozoic rocks of the West African Craton has been debated and various interpretations have emerged, even from the same area. In Ghana, for example, Leube et al. (1990) have proposed an intracontinental rift model for the Palaeoproterozoic rocks, whereas arc or subduction related models are preferred by some other workers (Asiedu et al., 2004; Attoh et al., 2006; Dampare et al., 2008; Dampare et al., 2005; Loh & Hirdes, 1999; Pohl & Carlson, 1993; Sylvester & Attoh, 1992). Feybesse et al. (2006) developed a metallogenesis model for the occurrence of gold deposits in Ghana which invoked a combination of continental margin, juvenile magmatism and convergence and collision between an old continent and a juvenile crust for the tectonic environments in which the Birimian greenstone belts were generated. In this context, the Ashanti volcanic belt is considered to mark the boundary between an Archaean continental domain and a Birimian oceanic domain. For Harcouët et al. (2007), the basement in the Ashanti area is likely to be of continental type rather than oceanic, as the results of their numerical modelling using thermal parameters such as thermal conductivity values and heat-production rates are more consistent with the continental basement scenario. Leube et al. (1990) have indicated that most Birimian tholeiites have N-MORB chemistry with few showing slight to moderate LREE enrichment. The authors interpret the coexistence of both flat and LREE-enriched patterns of tholeiites and also the ε_{Nd} value of +2 (Taylor, Moorbath, Leube, & Hirdes, 1988) as indications of slight crustal contamination in the petrogenesis of the tholeiites. For Sylvester and Attoh (1992), the trace element chemistry of Birimian volcanic belts in Ghana is comparable to that of Archaean greenstone belts, and that intermediate calc-alkaline units show the high Ba/La and Ta depletion which is characteristic of similar rocks in modern subduction environments and distinct from those formed in intraplate settings. The authors therefore suggest that Birimian volcanic rocks probably originated as immature island arcs built on oceanic crust. Dampare, Shibata, Asiedu, Okano, et al. (2008) have, on the basis of geochemistry, inferred an intra-oceanic island arc–fore-arc–back-arc setting for the Palaeoproterozoic metavolcanic rocks from the southern Ashanti volcanic belt. They recognize basalts with both flat to slightly LREE-depleted (N-MORB-like) and LREE-enriched patterns, and LREE-enriched calc-alkaline andesites in the volcanic suite, with the rocks displaying various degrees of subduction-related trace element characteristics. The formation of most of the Palaeoproterozoic volcanic belts in the oceanic context has also been proposed by other workers (e.g., Abouchami et al., 1990; Ama Salah, Liégeois, & Pouclet, 1996; Béziat et al., 2000; Boher et al., 1992; Davis et al., 1994; Egal et al., 2002; Liégeois et al., 1991; Vidal & Alric, 1994). Moreover, geochronological and isotopic data (e.g., Abouchami et al., 1990; Ama Salah et al., 1996; Boher et al., 1992; Doumbia et al., 1998; Gasquet et al., 2003; Hirdes et al., 1996; Liégeois et al., 1991; Taylor et al., 1992) indicate a juvenile source for the Palaeoproterozoic volcanic and granitic rocks, with the exceptions of plutons from the Winneba area in the southeast of Ghana (Taylor et al., 1992) and the vicinity of the Man nucleus (e.g., Kouamelan, Peucat, & Delor, 1997), where there is evidence of a stronger influence of recycled Archaean basement.

In terms of crustal growth event in the West African Craton, Abouchami et al. (1990) and Boher et al. (1992) proposed a mantle plume model, in which extensive plateaus were formed by a mantle plume event, followed by formation of island arcs on the top of the oceanic plateaus that then collided with the Man Archaean craton. In the case of Ghana, Taylor et al. (1992) have indicated, from geochronological and isotopic data, that the Birimian of Ghana represents a major Early Proterozoic magmatic crust-forming event around 2.3–2.0 Ga by differentiation from a slightly depleted mantle source. Thus, the Birimian of Ghana forms part of the major Proterozoic (Eburnean)

episode of juvenile crustal accretion which is recognized in West African Craton and dated at 2.2–2.1 by Abouchami et al. (1990). Davis et al. (1994), also following the accretionary model, have proposed that the Birimian sedimentary basins resulted from accretion of arcs and oceanic plateaus now represented by allochthonous Birimian volcanic belts.

Our present geochemical and isotopic data as well as field observations are inconsistent with the mantle plume model proposed for Palaeoproterozoic rocks in Ghana (e.g., Leube et al., 1990) but rather plead in favour of a supra-subduction setting in the study area. Magmatism associated with mantle plumes is usually voluminous, consists of basaltic lavas, high-Mg komatiites and picrites, and may be associated with radiating mafic dyke swarms (e.g., Park et al., 1995). Although some komatiites have been identified among the volcanic rocks in Ghana (Leube et al., 1990), they are generally insignificant in volume and are scarce in the southern Ashanti volcanic belt. Palaeoproterozoic igneous assemblages in the southern Ashanti belt include granitoids with volcanic-arc-like geochemical features (Loh & Hirdes, 1999; Dampare et al., 2005; this study). Thus, evidence for a Palaeoproterozoic mantle plume is lacking. The Palaeoproterozoic mafic and ultramafic rocks in the belt do not have OIB signatures, ruling out a plume-related origin. Instead, the source region was strongly modified by fluids and melts derived from a subducted slab. The question arises as to whether this modified mantle was a relic produced by older subduction or if subduction was coeval with production of the mafic magmas. An active subduction environment is consistent with the geology of the area, a back-arc volcanic sequence associated with the ophiolitic plutonics (Dampare, Shibata, Asiedu, Osae, & Banoeng-Yakubo, 2008). It is also known that some of the granitoid plutons in the region have adakitic affinities (this study), and such adakitic melts could have produced the enrichment of the mantle source region from which the some of the gabbros were derived. These observations support the interpretation that the intrusions were related to active subduction during the Palaeoproterozoic. Many subducted slabs experience multistage dehydration or melting (Rollinson & Tarney, 2005), which can occur separately in space and time (Elliott et al., 1997; Turner et al., 1997). Slab dehydration normally occurs at shallower depths than slab melting (Rollinson & Tarney, 2005). Slab melting (including sediment and altered basalt) is usually thought to be limited to young and relatively hot oceanic crust and typically produces adakitic (Stern & Kilian, 1996) and high-Mg andesitic magmas (e.g., Tsuchiya, Suzuki, Kimura, & Kagami, 2005). Thus, removal of mobile LILE from the slab by fluids is typically associated with the early stages of subduction, whereas later melting produces adakites with high K/Rb ratios and low Th, K, and Rb contents (Rollinson & Tarney, 2005; Stern & Kilian, 1996). Consequently, rocks associated with slab melt-modification are generally distributed behind those derived from fluid enriched mantle sources (Rollinson & Tarney, 2005). In the southern Ashanti belt, the close association of the gabbros and the granitoids, as well as the pyroxenites, suggests that both dehydration and slab melting occurred approximately simultaneous at the same crustal level. Therefore, we suggest that the subduction zone was steep, and the mantle was relatively warm due to convection at an active continental margin.

5.4 | Pre-Birimian (or Archaean?) crust in Ghana

As indicated earlier, the ε_{Nd} (2.1 Ga) values of the plutonic rocks range from −5.68 to +4.93, suggesting that the mantle source of the rocks have been contaminated to various degrees by crustal components. The Nd model ages (T_{DM2}), 1.99–2.75 Ga, provide further evidence for a pre-Birimian crust in the study area. The juvenile character or otherwise of the analysed rocks was visualized in the plot of ε_{Nd} (2.1 Ga) versus formation age (t; Figure 15). The Nd isotopic evolutionary trend of Archaean crust is also shown for comparison. The isotopic values used are from Kouamelan, Peucat, and Delor (1997), who estimated the composition of the Archaean rocks form Cote d'Ivoire which forms part of the Archaean domain of the WAC, since no Archaean crust is known in Ghana, at least for now. These Archaean rocks have ε_{Nd} (2.1 Ga) values ranging from −10 to −13. The metaperidotites from the Aketakyi ultramafic complex, Aketakyi gabbro, Prince's Town quartz diorite (D9023A), and the Kegyina gabbro (D90310) either fall in or close to the depleted mantle curve, which suggest that they were juvenile at their time of formation (Figure 15).

The Palaeoproterozoic Nd model ages (1.83–2.17 Ga; Table 5) of these rocks support their juvenile character. The Prince's Town granitoids (D9025 and D9038), Axim gabbro and Kegyina gabbro and Ahama pyroxenitic rocks are dominated by pre-Birimian (and Neoarchaean) Nd model ages of 2.41–2.51, 2.54–2.55, 2.39–2.57, and 2.52–2.75 Ga, respectively (Table 5). Their respective ε_{Nd} (2.1 Ga) values of −1.01 to +0.16, −1.23 to −1.17, −0.94 to +0.46, and −0.58 to −5.68 indicate variable contributions from pre-Birimian crustal materials, with the most significant contribution recorded in the Ahama pyroxenitic rocks. Thus, the Ahama pyroxenites show a clear evidence of older crustal/Archaean inputs, which is probably

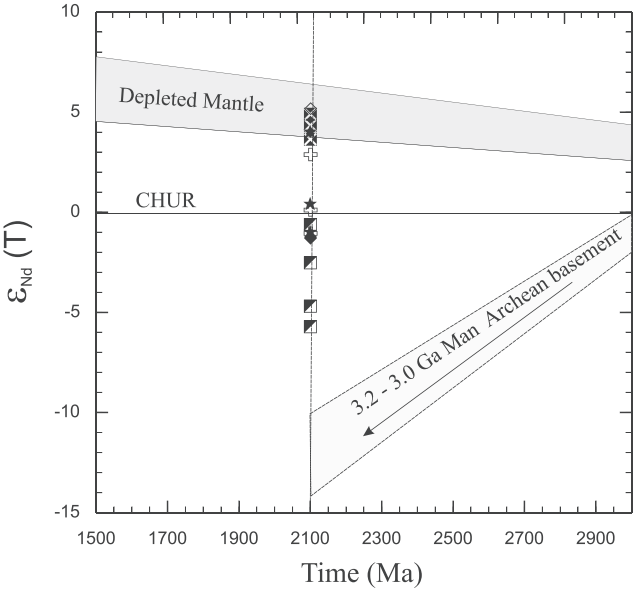

FIGURE 15 Plot of ε_{Nd} (2.1 Ga) versus formation age (time) for the Palaeoproterozoic rocks from the Ashanti volcanic belt. Data of Archaean continental crust is from Kouamelan, Peucat, and Delor (1997) CHUR = Chondritic uniform reservoir. Symbols as in Figure 14

supported by their ε_{Nd} (2.1 Ga) values being relatively closer to the Archaean crust, compared to the other rocks. The occurrence of some pre-Birimian ages in detrital zircons (2,245–2,266 Ma) from the Tarkwaian sediments (Davis et al., 1994; Loh & Hirdes, 1999) lends support to the pre-Birimian crustal growth episode in Ghana. These data are not exceptional to Ghana, as the occurrence of some pre-Birimian ages have also been reported in two zircon grains (2,208 and 2,220 Ma) from the Tafolo tonalite in central Cote d'Ivoire (Doumbia et al., 1998), in zircon cores from the Issia granite (2,212–2,305 Ma) in south-western Cote d'Ivoire (Kouamelan, 1996; Kouamelan, Peucat, & Delor, 1997), and in zircon cores from the Dabakala tonalite (2,312 ± 17 Ma) in central Cote d'Ivoire (Gasquet et al., 2003).

The Nd isotopic data provide evidence for a possible contamination of the juvenile Birimian crust of the southern Ashanti belt by a significant amount of a pre-Birimian crustal material. Does it indicate an Archaean crust beneath the southern Ashanti greenstone belt? Contrary to other isotopic studies on the Birimian rocks of Ghana (Taylor et al., 1992), which tend to preclude the involvement of notable contributions from an older crust in their genesis with the exception of the Winneba granitoids, the present data may implicate a recycled Archaean crustal material component in the genesis of some of the igneous rocks in the study area. The low initial $^{87}Sr/^{86}Sr$ ratios tend to argue against an Archaean terrane at lower crustal levels. Alternatively, the Archaean component might have resulted from subduction of sediments from Archaean cratons or small Archaean terranes. In this scenario, the retained strontium isotopic signature of the older crustal material could probably be similar to that of the plutonic rocks. This latter interpretation, where the Palaeoproterozoic mantle-derived rocks were contaminated by crustal materials derived from subduction, is favoured since the geochemistry of the rocks (including HFSE depletion) does not support major crustal contamination during magmatic emplacement and crystallization.

6 | CONCLUSIONS

The trace element signatures as well as the field relations of the studied granitoids and mafic–ultramafic rocks associated with metavolcanic rocks in the southern Ashanti greenstone belt have led to the conclusions presented below. The I-type Prince's Town granitoids show geochemical features characteristic of subduction-related granitoids as found worldwide in intra-oceanic arcs. The Ahama pyroxenites, Axim gabbro, and Kegyina gabbroic rocks are subduction-related ultramafic and mafic intrusions which occur in the Axim volcanic branch. These gabbroic and Ahama pyroxenitic rocks may have been derived from lithospheric mantle sources, with the Ahama pyroxenites being extracted from a more fluid-metasomatized mantle different from that of Axim and Kegyina and Aketakyi gabbroic. These rocks share similar characteristics with the LREE-enriched intra-oceanic-island arc-fore-arc basalts/basaltic andesites, which also occur in the Axim volcanic lobe (see Dampare, Shibata, Asiedu, Osae, & Banoeng-Yakubo, 2008).

The Aketakyi ultramafic complex demonstrates a supra-subduction affinity and is associated with the LREE-depleted, arc-like Aketakyi gabbro and the LREE-depleted, back-arc-basin basalts in the Cape Three Points volcanic branch. The ultramafic complex probably originated from a mafic magma in the greenstone belt of which the tholeiitic basalt is a possible candidate. Brown amphibole in the Aketakyi ultramafic complex shows postcumulus textural characteristics (i.e., postcumulus phase enclosing olivine, pyroxene, and serpentinized olivine grains). The occurrence of primary magmatic amphibole suggests the presence of relatively high water contents in the parental magma. Thus, hydrous partial melting of a mantle source which had previously been metasomatized is envisaged.

The analysed plutonic rocks commonly have low initial $^{87}Sr/^{86}Sr$ ratios consistent with previous studies on Palaeoproterozoic rocks from the West African Craton. The granitoids have ε_{Nd} (2.1 Ga) values ranging from −1.01 to +2.92 and T_{DM2} of 2.17–2.51 Ga, whereas the gabbros have ε_{Nd} (2.1 Ga) ranging from −1.23 to +5.23 and T_{DM2} values from 2.08 to 2.57 Ga. The Group I pyroxenites from the Ahama ultramafic body show negative initial ε_{Nd} (2.1 Ga) values from −0.58 to −2.48 and T_{DM2} values of 2.52 to 2.75 Ga, whereas the Group II pyroxenites show relatively higher negative ε_{Nd} (2.1 Ga) values ranging from −4.66 to −5.68 but no meaningful T_{DM2} ages. The metaperidotites from the Aketakyi ultramafic/ophiolitic complex show high positive ε_{Nd} (2.1 Ga) values from +3.69 to +4.93, and T_{DM2} values of 1.99 to 2.04 Ga, which suggest that they were juvenile at their time of formation. Their high positive ε_{Nd} (2.1 Ga) values suggest they derived from depleted mantle magmas.

The Nd isotopic data provide evidence for a possible contamination of the juvenile Birimian crust of the southern Ashanti belt by some amount of a pre-Birimian crustal material. The low initial $^{87}Sr/^{86}Sr$ ratios tend to argue against an Archaean terrane at lower crustal levels. Alternatively, the Archaean component might have resulted from subduction of sediments from Archaean cratons. This latter interpretation, where the Palaeoproterozoic mantle-derived rocks were contaminated by crustal materials derived from subduction, is favoured since the geochemistry of the rocks does not support major crustal contamination during magmatic emplacement and crystallization.

In conclusion, the ultramafic to mafic bodies and granitoid intrusives which are associated with metavolcanic rocks in the southern Ashanti greenstone belts of Ghana were not plume-generated but were derived through supra-subduction-related magmatism during the Palaeoproterozoic. This is consistent with the island arc complex model in which the Palaeoproterozoic terranes of West Africa evolved through subduction–accretion processes.

ACKNOWLEDGEMENTS

Field work was sponsored by the National Nuclear Research Institute (NNRI) of the Ghana Atomic Energy Commission (GAEC). The first author gratefully acknowledges the financial support provided by the Japanese Government (Monbukagakusho: MEXT) and Okayama University for laboratory work. The XRF analyses were performed at the

Department of Earth Sciences, Okayama University, Japan, with the assistance of Ms. Mayumi Usui. Critical comments by anonymous reviewers are gratefully appreciated.

ORCID

Samuel B. Dampare https://orcid.org/0000-0002-7314-9581
Patrick A. Sakyi https://orcid.org/0000-0002-7536-6264

REFERENCES

Abouchami, W., Boher, M., Michard, A., & Albarede, F. (1990). A major 2.1 Ga event of mantle magmatism in West Africa: An early stage of crustal accretion. *Journal of Geophysical Research*, *95*, 17605–17629. https://doi.org/10.1029/JB095iB11p17605

Albarède, F., & Brouxel, M. (1987). The Sm–Nd secular evolution of the continental crust and the depleted mantle. *Earth and Planetary Science Letters*, *82*, 25–36. https://doi.org/10.1016/0012-821X(87)90104-X

Allibone, A., McCuaig, C. T., Harris, D., Etheridge, M., Munroe, S., Byrne, D., … Gyapong, W. (2002). Structural controls on gold mineralization at the Ashanti Gold Deposit, Obuasi, Ghana. In R. J. Goldfarb, & R. L. Neilson (Eds.), *Integrated methods for discovery: Global exploration in the 21st century* (Vol. 9). *Society of Economic Geologists Special Publication*. (pp. 65–93). Littleton: Society of Economic Geologists, Inc. (SEG).

Altherr, R., Holl, A., Hegner, E., Langer, C., & Kreuzer, H. (2000). High potassium, calc-alkaline I-type plutonism in the European Variscides: northern Vosges (France) and northern Schwarzwald (Germany). *Lithos 50*, 51–73.

Ama Salah, I., Liégeois, J.-P., & Pouclet, A. (1996). Evolution d'un arc insulaire océanique birimian précoce au Liptako nigérien (Sirba): géologie, géochronologie et géochimie. *Journal of African Earth Sciences*, *22*(3), 235–254. https://doi.org/10.1016/0899-5362(96)00016-4

Asiedu, D. K., Dampare, S. B., Asamoah, S. P., Banoeng-Yakubo, B., Osae, S., Nyarko, B. J. B., & Manu, J. (2004). Geochemistry of Paleoproterozoic metasedimentary rocks from the Birim diamondiferous field, southern Ghana: Implications for provenance and crustal evolution at the Archean–Proterozoic boundary. *Geochemical Journal*, *38*, 215–228. https://doi.org/10.2343/geochemj.38.215

Atherton, M. P., & Petford, N. (1993). Generation of sodium-rich magmas from newly underplated basaltic crust. *Nature*, *362*, 144–146. https://doi.org/10.1038/362144a0

Attoh, K., & Ekwueme, B. (1997). The West African shield. In M. J. De Wit, & L. D. Ashwall (Eds.), *Greenstone belts* (pp. 517–528). New York: Oxford University Press.

Attoh, K., Evans, M. J., & Bickford, M. E. (2006). Geochemistry of an ultramafic-rodingite rock association in the Paleoproterozoic Dixcove greenstone belt, southwestern Ghana. *Journal of African Earth Sciences*, *45*, 333–346. https://doi.org/10.1016/j.jafrearsci.2006.03.010

Bach, W., Hegner, E., & Erzinger, J. (1998). Chemical fluxes in the Tonga subduction zone: Evidence from the southern Lau Basin. *Geophysical Research Letters*, *25*, 1467–1470. https://doi.org/10.1029/98GL00840

Barnes, S.-J., Naldrett, A. J., & Gorton, M. P. (1985). The origin of the fractionation of platinum-group elements in terrestrial magmas. *Chemical Geology*, *53*, 303–323.

Bartholomew, R. W. (1961). The geology of 1/4° field sheets 3 and 5 Axim NE,1. *Ghana Geological Survey Arch Rep*, *18*(1991), 78.

Bassot, J. P. (1987). Le complexe volcano-plutonique calcoalcalin de la rive're Daléma (Est Sénegal): Discussion de sa signification géodynamique dans le cadre de l'orogénie eburnéenne (Protérozoic inférieur). *Journal of African Earth Sciences*, *6*(4), 505–519. https://doi.org/10.1016/0899-5362(87)90091-1

Batchelor, B., & Bowden, P. (1985). Petrogenetic interpretation of granitoid rock series using multicationic parameters. *Chemical Geology*, *48*, 43–55. https://doi.org/10.1016/0009-2541(85)90034-8

Ben Othman, D., Polvé, M., & Allègre, C. J. (1984). Nd–Sr isotopic composition of granulites and constraints on the evolution of the lower continental crust. *Nature*, *307*, 510–515. https://doi.org/10.1038/307510a0

Bessoles, B. (1977). Geologie de l'Afrique: le craton ouest-African. *Memoire BRGM*, *88*, 403.

Béziat, D., Bourges, F., Debat, P., Lompo, M., Martin, F., & Tollon, F. (2000). A paleoproterozoic ultramafic-mafic assemblage and associated volcanic rocks of the Boromo greenstone belt: Fractionates originating from island-arc volcanic activity in the West African craton. *Precambrian Research*, *101*, 25–47. https://doi.org/10.1016/S0301-9268(99)00085-6

Béziat, D., Dubois, M., Debat, P., Nikiema, S., Salvi, S., & Tollon, F. (2008). Gold metallogeny in the Birimian craton of Burkina Faso (West Africa). *Journal of Earth Science*, *50*, 215–233.

Blenkinsop, T. G., Schmidt-Mumm, A., Kumi, R., & Sangmor, S. (1994). Structural geology of the Ashanti gold mine, Obuasi, Ghana. *Geological Jahrbuch*, *D100*, 131–153.

Boher, M., Abouchami, W., Michard, A., Albarède, F., & Arndt, N. T. (1992). Crustal growth in West Africa at 2.1 Ga. *Journal of Geophysical Research*, *97*, 345–369. https://doi.org/10.1029/91JB01640

Bonatti, E., & Michael, P. J. (1989). Mantle peridotites from continental rifts to ocean basins to subduction zones. *Earth and Planetary Science Letters*, *91*, 297–311. https://doi.org/10.1016/0012-821X(89)90005-8

Castillo, R. P., Janney, P. E., & Solidum, R. S. (1999). Petrology and geochemistry of Camiguia Island, Southern Phillippines: Insight to the source of adakites and other lavas in a complex arc setting. *Contributions Mineralogy and Petrology*, *134*, 33–51.

Class, C., Miller, D. M., Goldstein, S. L., & Langmuir, C. H. (2000). Distinguishing melt and fluid subduction components in Umnak Volcanics, Aleutian Arc. *Geochemistry, Geophysics, Geosystems*, *1*, 1–28.

Coleman, R. G. (1977). *Ophiolites: Ancient oceanic lithosphere?* (p. 229). New York: Springer-Verlag. https://doi.org/10.1007/978-3-642-66673-5

Dampare, S., Shibata, T., Asiedu, D., & Osae, H. (2005). Major-element geochemistry of Proterozoic Prince's Town granitoid from the southern Ashanti volcanic belt, Ghana. *Okayama University Earth Science Reports*, *12*, 15–30.

Dampare, S. B., Shibata, T., Asiedu, D. K., Okano, O., Manu, J., & Sakyi, P. (2008). Sr–Nd isotopic compositions of Paleoproterozoic metavolcanic rocks from the southern Ashanti volcanic belt, Ghana. *Okayama University Earth Science Reports*, *16*, 9–28.

Dampare, S. B., Shibata, T., Asiedu, D. K., Osae, S., & Banoeng-Yakubo, B. (2008). Geochemistry of Paleoproterozoic metavolcanic rocks from the southern Ashanti volcanic belt, Ghana: Petrogenetic and tectonic setting implications. *Precambrian Research*, *162*, 403–423.

Davis, D. W., Hirdes, W., Schaltegger, U., & Nunoo, E. A. (1994). U–Pb age constraints on deposition and provenance of Birimian and gold-bearing Tarkwaian sediments in Ghana, West Africa. *Precambrian Research*, *67*, 89–107. https://doi.org/10.1016/0301-9268(94)90006-X

Debat, P., Nikiema, S., Mercier, A., Lompo, M., Beziat, D., Bourges, F., … Wenmenga, U. (2003). A new metamorphic constraint for the Eburnean orogeny from Paleoproterozoic formations of the Man shield (Aribinda and Tampelga countries, Burkina Faso). *Precambrian Research*, *123*, 47–65. https://doi.org/10.1016/S0301-9268(03)00046-9

Defant, M. J., & Drummond, M. S. (1990). Derivation of some modern arc magmas by melting of young subducted lithosphere. *Nature*, *347*, 662–665. https://doi.org/10.1038/347662a0

DePaolo, D. J. (1981). Neodymium isotopes in the Colorado Front Range and crust-mantle evolution in the Proterozoic. *Nature (London)*, *291*, 193–196. https://doi.org/10.1038/291193a0

DePaolo, D. J., Linn, A. M., & Schubert, G. (1991). The continental crust age distribution: Methods of determining mantle separation ages from Sm–Nd isotopic data and implication to the southwestern United States. *Journal of Geophysical Research*, *96*(B2), 2071–2088. https://doi.org/10.1029/90JB02219

Doumbia, S., Pouclet, A., Kouamelan, A., Peucat, J. J., Vidal, M., & Delor, C. (1998). Petrogenesis of juvenile-type Birimian (Palaeoproterozoic) granitoids in Central Côte d'Ivoire, West Africa: Geochemistry and Geochronology. *Precambrian Research*, *87*, 33–63.

Edwards, C. M. H., Menzies, M. A., Thirlwall, M. F., Morris, J. D., Leeman, W. P., & Harmon, R. S. (1994). The transition to potassic alkaline volcanism in island arcs: The Ringgit-Beser complex, east Java, Indonesia. *Journal of Petrology*, *35*, 1557–1595. https://doi.org/10.1093/petrology/35.6.1557

Egal, E., Thiéblemont, D., Lahondère, D., Guerrot, C., Costea, C. A., Iliescu, D., … Kolié, P. (2002). Late Eburnean granitization and tectonics along the western and northwestern margin of the Archean Kénéma–Man domain (Guinea, West African Craton). *Precambrian Research*, *117*, 57–84. https://doi.org/10.1016/S0301-9268(02)00060-8

Eisenlohr, B. N. (1989). Conflicting evidence on the timing of mesothermal and paleoplacer gold mineralisation in early Proterozoic rocks from southwest Ghana, West Africa. *Mineral Deposita*, *27*, 23–29.

Eisenlohr, B. N., & Hirdes, W. (1992). The structural development of the early Proterozoic Birimian and Tarkwaian rocks of southwest Ghana, West Africa. *Journal of African Earth Sciences*, *14*, 313–325. https://doi.org/10.1016/0899-5362(92)90035-B

Elliott, T., Plank, T., Zindler, A., White, W., & Bourdon, B. (1997). Element transport from slab to volcanic front at the Mariana arc. *Journal of Geophysical Research*, *102*, 14991–15019. https://doi.org/10.1029/97JB00788

Feybesse, J. L., Billa, M., Guerrot, C., Duguey, E., Lescuyer, J. L., Jean-Pierre Milési, J. P., & Bouchot, V. (2006). The paleoproterozoic Ghanaian province: Geodynamic model and ore controls, including regional stress modeling. *Precambrian Research*, *149*, 149–196. https://doi.org/10.1016/j.precamres.2006.06.003

Feybesse, J. L., & Milési, J. P. (1994). The Archean/proterozoic contact zone in West Africa: A mountain belt of décollement thrusting and folding on a continental margin related to 2.1 Ga convergence of Archean cratons? *Precambrian Research*, *69*, 199–227. https://doi.org/10.1016/0301-9268(94)90087-6

Gasquet, D., Barbey, P., Adou, M., & Paquette, J. L. (2003). Structure, Sr–Nd isotope geochemistry and zircon U–Pb geochronology of the granitoids of the Dabakala area (Côte d'Ivoire): Evidence for a 2.3 Ga crustal growth event in the Paleoproterozoic of West Africa? *Precambrian Research*, *127*, 329–354. https://doi.org/10.1016/S0301-9268(03)00209-2

Goldstein, S. L., O'Nions, R. K., & Hamilton, P. J. (1984). A Sm–Nd isotopic study of atmospheric dusts and particulate from major river systems. *Earth and Planetary Science Letters*, *70*, 221–236. https://doi.org/10.1016/0012-821X(84)90007-4

Grove, T. L., Parman, S. W., Bowring, S. A., Price, R. C., & Baker, M. B. (2002). The role of an H_2O-rich fluid component in the generation of primitive basaltic andesites and andesites form the Mt. Shasta region, N. California. *Contributions to Mineralogy and Petrology*, *142*, 375–396. https://doi.org/10.1007/s004100100299

Harcouët, V., Guillou-Frottier, L., Bonneville, A., Bouchot, V., & Milesi, J.-P. (2007). Geological and thermal conditions before the major Palaeoproterozoic gold-mineralization event at Ashanti, Ghana, as inferred from improved thermal modeling. *Precambrian Research*, *154*, 71–87. https://doi.org/10.1016/j.precamres.2006.11.014

Hart, S. R., & Dune, T. (1993). Experimental cpx/melt partitioning of 24 trace elements. *Contributions to Mineralogy and Petrology*, *113*, 1–8. https://doi.org/10.1007/BF00320827

Hawkesworth, C. J., Turner, S. P., McDermott, F., Peate, D. W., & van Calsteren, P. (1997). U–Th isotopes in arc magmas: Implication for element transfer from the subducted crust. *Science*, *276*, 551–555. https://doi.org/10.1126/science.276.5312.551

Hirdes, W., & Davis, D. W. (2002). U–Pb geochronology of Paleoproterozoic rocks in the southern part of the Keougou-Keneba inlier, Senegal, West Africa: Evidence for diachronous accretionary development of the Birimian Province. *Precambrian Research*, *118*, 83–99.

Hirdes, W., Davis, D. W., & Eisenlohr, B. N. (1992). Reassessment of Proterozoic of Proterozoic granitoid ages in Ghana on the basis of U/Pb zircon and monzanite dating. *Precambrian Research*, *56*, 89–96. https://doi.org/10.1016/0301-9268(92)90085-3

Hirdes, W., Davis, D. W., Lüdtke, G., & Konan, G. (1996). Two generations of Birimian (Paleoproterozoic) volcanic belts in northeastern Côte d'Ivoire (West Africa): Consequences for the 'Birimian controversy'. *Precambrian Research*, *80*, 173–191. https://doi.org/10.1016/S0301-9268(96)00011-3

Hofmann, A. W. (2003). Sampling mantle heterogeneity through oceanic basalts: Isotopes and trace elements. In R. W. Carlson (Ed.) *The Mantle and Core* (Vol. 2). (pp. 61–101). Elsevier: New York.

Jenner, G. A., Cawood, P. A., Rautenschlein, M., & White, W. M. (1987). Composition of backarc basin volcanics, Valu Fa Ridge, Lau Basin: Evidence for a slab-derived component in their mantle source. *Journal of Volcanology and Hydrothermal Research*, *32*, 209–222. https://doi.org/10.1016/0377-0273(87)90045-X

John, T., Klemd, R., Hirdes, W., & Loh, G. (1999). The metamorphic evolution of the paleoproterozoic (Birimian) volcanic Ashanti belt (Ghana, West Africa). *Precambrian Research*, *98*, 11–30. https://doi.org/10.1016/S0301-9268(99)00024-8

Johnson, K. T. M. (1998). Experimental determination of partition coefficients for rare earth and high-field-strength elements between clinopyroxene, garnet, and basaltic melt at high pressure. *Contributions to Mineralogy and Petrology*, *133*, 60–68. https://doi.org/10.1007/s004100050437

Junner, N. R. (1940). Geology of the Gold Coast and Western Togoland. *Gold Coast Geological Survey Bulletin*, *11*, 40.

Kay, R. W., & Mahlburg Kay, S. (1993). Delamination and delamination magmatism. *Tectonophysics*, *219*, 177–189. https://doi.org/10.1016/0040-1951(93)90295-U

Kepezhinskas, P., McDermott, F., Defant, M., Hochstaedter, A., Drummond, M. S., Hawdesworth, C. J., … Bellon, H. (1997). Trace element and Sr–Nd–Pb isotopic constraints on a three-component model of Kamchatka Arc petrogenesis. *Geochimica et Cosmochimica Acta*, *61*, 577–600. https://doi.org/10.1016/S0016-7037(96)00349-3

Keppler, H. (1996). Constraints from partitioning experiments on the composition of subduction-zone fluids. *Nature*, *380*, 237–240. https://doi.org/10.1038/380237a0

Keto, L. S., & Jacobsen, S. B. (1987). Nd and Sr isotopic variations of early Paleozoic oceans. *Earth and Planetary Science Letters*, *84*, 27–41. https://doi.org/10.1016/0012-821X(87)90173-7

Kouamelan, A. N. (1996). Géochronologie et géochime des formations archéennes et protérozoïques de la dorsale de Man en Côte d'Ivoire.

Implications Pour la Transition Archéen-Protérozoïque. Mém. Géosciences Rennes, *73*, 290.

Kouamelan, A. N., Delor, C., & Peucat, J.-J. (1997). Geochronological evidence for reworking of Archean terrains during the Early Proterozoic (2.1 Ga) in the western Cote d'Ivoire (Man Rise-West African Craton). *Precambrian Research*, *86*, 177–199. https://doi.org/10.1016/S0301-9268(97)00043-0

Kouamelan, A. N., Peucat, J. J., & Delor, C. (1997). Reliques archéennes (3,15 Ga) au sein du magmatisme birimien (2,1 Ga) de Côte d'Ivoire, craton Ouest-African. *Comptes rendus de l'Académie des sciences. Série 2. Sciences de la terre et des planètes*, *324*(9), 719–727.

Ledru, P., Johan, V., Milési, J. P., & Tegyey, M. (1994). Markers of the last stages of the Palaeoproterozoic collision: evidence for a 2 Ga continent involving circum-South Atlantic provinces. *Precambrian Research*, *69*, 169–191. https://doi.org/10.1016/0301-9268(94)90085-X

Lemoine, S., 1988. *Evolution géologique de la région de Dabakala (NE Côte d'Ivoire) au Protérozoïque inférieur. Unpublished thesis, Univ. Clermont-Ferrand*, 338 p.

Leube, A., Hirdes, W., Mauer, R., & Kesse, G. O. (1990). The early Proterozoic Birimian Supergroup of Ghana and some aspects of its associated gold mineralization. *Precambrian Research*, *46*, 139–165. https://doi.org/10.1016/0301-9268(90)90070-7

Liégeois, J. P., Claessens, W., Camara, D., & Klerkx, J. (1991). Short-lived Eburnian orogeny in southern Mali. Geology, tectonics, U–Pb and Rb–Sr geochronology. *Precambrian Research*, *50*, 111–136. https://doi.org/10.1016/0301-9268(91)90050-K

Loh, G., & Hirdes, W. (1999). Explanatory notes for the geological map of southwest Ghana 1:100,000: sheets Sekondi (0402A) and Axim (0403B): Ghana. *Geological Survey Bulletin*, *49*, 149.

Lompo, M. (2009). Geodynamic evolution of the 2.25–2.0 Ga Palaeoproterozoic magmatic rocks in the Man-Leo Shield of the West African Craton. A model of subsidence of an oceanic plateau. In S. M. Reddy, R. Mazumder, D. A. D. Evans, & A. S. Collins (Eds.), *Palaeoproterozoic supercontinents and global evolution* (Vol. 323). *Geological Society of London Special Publication*. (pp. 231–254). London: Geological Society.

Maniar, P. D., & Piccoli, P. M. (1989). Tectonic discrimination of granitoids. *Geological Society of America Bulletin*, *101*, 635–643. https://doi.org/10.1130/0016-7606(1989)101<0635:TDOG>2.3.CO;2

Martin, H., Smithies, R. H., Rapp, R., Moyen, J.-F., & Champion, D. (2005). *An overview of adakite, tonalite–trondhjemite–granodiorite (TTG), and sanukitoid: relationships and some implications for crustal evolution*. Lithos, 79, 1–24. https://doi.org/10.1016/j.lithos.2004.04.048

Mauer, R. (1990). *Petrographische und geochemische Unttersuchungen der präkambrischen (Birimian) Granitoide Ghanas. Diss. Techn. Univ. Berlin*, 202 pp.

McCulloch, M. T. (1987). Sm–Nd isotopic constraints on the evolution of Precambrian crust in the Australian continent. In A. Kröner (Ed.), *Proterozoic lithospheric evolution* (Vol. 17). *Geodyn. Series*. (pp. 115–130). Washington, D.C.: AGU.

McDonough, W.F., Frey, F.A., (1989). Rare earth elements in upper mantle rocks. In: Lipin, B., McKay, G. (Eds.), *Geochemistry and mineralogy of rare earth elements*. Reviews in Mineralogy vol. 21, pp. (99–145). Washington: The Mineralogical Society of America.

Milési, J. P., Ledru, P., Feybesse, J. L., Dommanget, A., & Marcoux, E. (1992). Early Proterozoic ore deposits and tectonics of the Birimian orogenic belt, West Africa. *Precambrian Research*, *58*, 305–344. https://doi.org/10.1016/0301-9268(92)90123-6

Miyashiro, A. (1974). Volcanic rock series in island arcs and active continental margins. *American Journal of Science*, *274*, 321–355. https://doi.org/10.2475/ajs.274.4.321

Mortimer, J. (1992). Lithostratigraphy of the early Proterozoic Toumodi Volcanic Group in Central Côte d'Ivoire: Implications for Birimian stratigraphy models. *Journal of African Earth Sciences*, *14*, 81–91. https://doi.org/10.1016/0899-5362(92)90057-J

Münker, C. (2000). The isotope and trace element budget of the Cambrian Devil River Arc System, New Zealand: Identification of four source components. *Journal of Petrology*, *41*, 759–788. https://doi.org/10.1093/petrology/41.6.759

Nelson, B. K., & DePaolo, D. J. (1985). Rapid production of continental crust 1.7 to 1.9 b.y. ago: Nd isotopic evidence from the basement of the North America mid continent. *Geological Society of America Bulletin*, *96*, 746–754. https://doi.org/10.1130/0016-7606(1985)96<746:RPOCCT>2.0.CO;2

Nesbitt, H. W., & Young, G. M. (1982). Early Proterozoic climates and plate motions inferred from major element chemistry of lutites. *Nature*, *299*, 715–717.

Oberthür, T., Vetter, U., Davis, D. W., & Amanor, J. A. (1998). Age constraints on gold mineralization and Palaeoproterozoic crystal evolution in the Ashanti belt of southern Ghana. *Precambrian Research*, *89*, 129–143.

Opare-Addo, E., John, B. E., Mukasa, S. B., & Browning, P. (1993). Field and geochronologic (U–Pb) constraints on the age and generation of granitoids and migmatites in southern Ghana. *EOS Transactions of American Geophysical Union*, *74*, S301.

Park, J. K., Buchan, K. L., & Harlan, S. S. (1995). A proposed giant radiating dyke swarm fragmented by the separation of Laurentia and Australia based on paleomagnetism of ca. 780 Ma mafic intrusions in western North America. *Earth and Planetary Science Letters*, *132*, 129–139.

Pawlig, S., Gueye, M., Klischies, R., Schwarz, S., Wemmer, K., & Siegesmund, S. (2006). Geochemical and Sr–Nd isotopic data on the Birimian of the Kedougou-Kenieba Inlier (Eastern Senegal): Implications on the Palaeoproterozoic evolution of the West African Craton. *South African Journal of Geology*, *109*, 411–427. https://doi.org/10.2113/gssajg.109.3.411

Peacock, S. M., Rushmer, T., & Thompson, A. B. (1994). Partial melting of subducting oceanic crust. *Earth and Planetary Science Letters*, *121*, 227–244. https://doi.org/10.1016/0012-821X(94)90042-6

Pearce, J. A., Harris, N. B. W., & Tindle, A. G. (1984). Trace element discrimination diagrams for the interpretation of granitic rocks. *Journal of Petrology*, *25*, 956–983. https://doi.org/10.1093/petrology/25.4.956

Pearce, J. A., & Norry, M. J. (1979). Petrogenetic implications of Ti, Zr, Y, and Nb, variation in volcanic rocks. *Contributions to Mineralogy and Petrology*, *69*, 33–47. https://doi.org/10.1007/BF00375192

Pearce, J. A., & Peate, D. W. (1995). Tectonic implications of the composition of volcanic arc magmas. *Annual Review of Earth and Planetary Sciences*, *23*, 251–285. https://doi.org/10.1146/annurev.ea.23.050195.001343

Petford, N., Atherton, M. P., & Halliday, A. N. (1996). Rapid magma production rates, underplating and remelting in the Andes: Isotopic evidence from northern-central Peru (90–110 s). *Journal of South American Earth Sciences*, *9*, 69–78. https://doi.org/10.1016/0895-9811(96)00028-4

Pigois, J.-P., Groves, D. I., Fletcher, I. R., McNaughton, N. J., & Snee, L. W. (2003). Age constraints on Tarkwaian palaeoplacer and lode-gold formation in the Tarkwa-Damang district, SW Ghana. *Mineralium Deposita*, *38*, 695–714. https://doi.org/10.1007/s00126-003-0360-5

Plank, T., & Langmuir, C. H. (1992). Sediments melt and basaltic crust dehydrates at subduction zones. *Eos, Transactions, American Geophysical Union*, *73*, 637.

Plank, T., & White, W. M. (1995). Nb and Ta in arc and mid-ocean basalts. *Eos*, *76*, 655.

Pohl, D., & Carlson, C. (1993). A plate tectonic re-interpretation of the 2.2–2.0 Ga Birimian province, Tarkwaian System and metallogenesis in West Africa. In J. W. Peters, G. O. Kesse, & Acquah (Eds.), *Regional trends in African geology* (pp. 378–381). Accra: Geological Society of Africa.

Qu, X. M., Hou, Z. Q., & Li, Y. G. (2004). Melt components derived from a subducted slab in late orogenic ore-bearing porphyries in the Gangdese copper belt, southern Tibetau plateau. *Lithos*, *74*, 131–148. https://doi.org/10.1016/j.lithos.2004.01.003

Roeder, P. L., & Elmslie, R. F. (1970). Olivine-liquid equilibrium. *Contributions to mineralogy and petrology*, *29*, 275–289. https://doi.org/10.1007/BF00371276

Roddaz, M., Debat, P., & Nikiéma, S. (2007). Geochemistry of Upper Birimian sediments (major and trace elements and Nd—Sr isotopes) and implications for weathering and tectonic setting of the Late Paleoproterozoic crust. *Precambrian Research*, *159*, 197–211.

Rollinson, H. R., & Tarney, J. (2005). Adakites—The key to understanding LILE depletion in granulites. *Lithos*, *79*, 61–81. https://doi.org/10.1016/j.lithos.2004.04.050

Stern, C. R., & Kilian, R. (1996). Role of the subducted slab, mantle wedge and continental crust in the generation of adakites from the Austral Volcanic Zone. *Contributions to Mineralogy and Petrology*, *123*, 263–281. https://doi.org/10.1007/s004100050155

Stolper, E., & Newman, S. (1994). The role of water in the petrogenesis of Mariana trough magmas. *Earth and Planetary Science Letters*, *121*, 293–325. https://doi.org/10.1016/0012-821X(94)90074-4

Sun, S. S., & McDonough, W. F. (1989). Chemical and isotopic systematics of oceanic basalts: Implication for mantle composition and processes. In A. D. Saunders, & M. J. Norry (Eds.), *Magmatism in ocean basins* (Vol. 42). *Geological Society of London Special Publication*. (pp. 313–345). London: Geological Society.

Sylvester, P. J., & Attoh, K. (1992). *Lithostratigraphy and composition of 2.1 Ga greenstone belts of the West African craton and their bearing on crustal evolution and Archean-Proterozoic boundary*. Journal of Geology, 100, 377–393. https://doi.org/10.1086/629593

Tagini, B. (1971). *Esquisse structurale de la Cote d'Ivoire. Essai de géotectonique régionale. These Univ. Lausanne. Soc. Dev. Min. Cote d'Ivoire (SODEMI)*, 302 pp.

Taylor, N. P., Moorbath, S., Leube, A., & Hirdes, W. (1992). Early Proterozoic crustal evolution in the Birimian of Ghana: Constraints from geochronology and isotope geochemistry. *Precambrian Research*, *56*, 97–111. https://doi.org/10.1016/0301-9268(92)90086-4

Taylor, P.N., Moorbath, S., Leube, A., & Hirdes, W. (1988). Geochronology and crustal evolution of Early Proterozoic granite-greenstone terrains in Ghana/West Africa. Abstract, International Conference on the geology of Ghana with special emphasis on Gold. 75th Anniversary of Ghana Geol. Surv. Dept., Accra, pp. 43–45.

Taylor, S. R., & McLennan, S. M. (1985). *The continental crust: Its composition and evolution* (p. 312). Oxford: Blackwell Scientific.

Tsuchiya, N., Suzuki, S., Kimura, J. I., & Kagami, H. (2005). Evidence for slab melt/mantle reaction: petrogenesis of Early Cretaceous and Eocene high-Mg andesites from the Kitakami Mountains, Japan. *Lithos*, *79*, 179–206. https://doi.org/10.1016/j.lithos.2004.04.053

Tunks, A. J., Selley, D., Rogers, J. R., & Brabham, G. (2004). Vein mineralization at the Damang Gold Mine, Ghana: Controls on mineralization. *Journal of Structural Geology*, *26*, 1257–1273. https://doi.org/10.1016/j.jsg.2003.11.005

Turner, S., Hawkesworth, C., Rogers, N., Barlett, J., Worthington, T., Hergt, J., … Smith, I. (1997). ^{238}U–^{230}Th disequilibria magma petrogenesis, and flux rates beneath the depleted Tonga–Kermadec island arc. *Geochimica et Cosmochimica Acta*, *61*, 4855–4884. https://doi.org/10.1016/S0016-7037(97)00281-0

Vidal, M., & Alric, G. (1994). The Palaeoproterozoic (Birimian) of Haute-Comoé in the West African craton, Ivory Coast: A transtensional back-arc basin. *Precambrian Research*, *65*, 207–229.

Wang, Q., Xu, J. F., Jian, P., Bao, Z. W., Zhao, Z. H., Li, C. F., … Ma, J. L. (2006). Petrogenesis of adakitic porphyries in an extensional tectonic setting, Dexing, south China: Implications for the genesis of porphyry copper mineralization. *Journal of Petrology*, *47*, 119–144. https://doi.org/10.1093/petrology/egi070

Weaver, B. L. (1990). Geochemistry of highly-undersaturated ocean island basalt suites from the South Atlantic Ocean: Fernando de Noronha and Trinidade islands. *Contributions to Mineralogy and Petrology*, *105*, 502–515. https://doi.org/10.1007/BF00302491

Wedepohl, K. H. (1995). The composition of the continental crust. *Geochimica et Cosmochimica Acta*, *59*, 1217–1232.

Whalen, J. B., Syme, E. C., & Stern, R. A. (1999). Geochemical and Nd isotopic evolution of Paleoproterozoic arc-type granitoid magmatism in the Flin Flon Belt, Trans-Hudson orogen, Canada. *Canadian Journal of Earth Sciences*, *36*, 227–250. https://doi.org/10.1139/e98-026

Woodhead, J. D., Eggins, S., & Gamble, J. (1993). High field strength and transition element systematics in island arc and back-arc basin basalts: Evidence for a multiphase melts extraction and a depleted mantle wedge. *Earth and Planetary Science Letters*, *144*, 491–504.

Wu, F., Zhao, G., Simon, A., Wilde, S. A., & Sun, D. (2005). Nd isotopic constraints on crustal formation in the North China Craton. *Journal of Asian Earth Sciences*, *24*, 523–545. https://doi.org/10.1016/j.jseaes.2003.10.011

Yao, Y., Murphy, P. J., & Robb, L. J. (2001). Fluid characteristics of granitoid-hosted gold deposits in the Birimian terrane of Ghana: A fluid inclusion microthermometric and Raman spectroscopic study. *Economic Geology*, *96*, 1611–1643.

Zhao, J.-H., & Zhou, M.-F. (2007). Geochemistry of Neoproterozoic mafic intrusions in the Panzhihua district (Sichuan Province, SW China): Implications for subduction-related metasomatism in the upper mantle. *Precambrian Research*, *152*, 27–47. https://doi.org/10.1016/j.precamres.2006.09.002

Zhou, M.-F., Kennedy, A. K., Sun, M., Malpas, J., & Lesher, C. M. (2002). Neo-proterozoic arc-related mafic intrusions in the northern margin of South China: implications for accretion of Rodinia. *Journal of Geology*, *110*, 611–618. https://doi.org/10.1086/341762

Zou, H. B., Zindler, A., Xu, X. S., & Qu, Q. (2000). Major, trace element, and Nd, Sr and Pb isotope studies of Cenozoic basalts in SE China: Mantle sources, regional variations, and tectonic significance. *Chemical Geology*, *171*, 33–47. https://doi.org/10.1016/S0009-2541(00)00243-6

How to cite this article: Dampare SB, Shibata T, Asiedu DK, et al. Ultramafic–mafic and granitoids supra-subduction magmatism in the southern Ashanti volcanic belt, Ghana: Evidence from geochemistry and Nd isotopes. *Geological Journal*. 2019;1–37. https://doi.org/10.1002/gj.3512

APPENDIX A
ANALYTICAL TECHNIQUES

Major and trace element analyses

Samples were collected from mafic, ultramafic, and granitoid outcrops associated with metavolcanic rocks in the Axim and Cape Three Points volcanic branches of the southern Ashanti greenstone belt. Analysis of major elements was carried out on fused discs by the automated X-ray fluorescence spectrometer, Philips model PW 1480, at the Department of Earth Sciences, Okayama University. All samples were crushed and milled in an agate mortar as tungsten carbide crushing/milling vessels are a well-known source of Ta contamination. The procedure for preparation of glass beads for X-ray fluorescence (XRF) analysis, analytical techniques, and quality control on the XRF analyses are described elsewhere (Dampare, Shibata, Asiedu, Osae, & Banoeng-Yakubo, 2008). The precision was generally better than 1%. Loss on ignition (LOI) was computed from weight loss by heating an oven-dried (110°C) whole-rock powder to 1000°C for 2 hr.

The trace elements analyses selected samples were performed at the Activation Laboratories Ltd. (Actlabs), Ontario, Canada, using fusion inductively coupled plasma and inductively coupled plasma-mass spectrometry (ICP-MS). In all, 26 samples collected from the granitoid intrusion and various mafic and/or ultramafic bodies in the study area were selected, taking into consideration the level of alteration, as indicated by their LOI values. Details of the analytical procedure (i.e., accuracy, precision, and standards) can be obtained from the Activation Laboratories Ltd. The detection limits (in ppm) for the measured trace elements are 5 (V, As, Pb), 20 (Cr, Ni), 1 (Co, Ga, Rb, Zr, Sn), 10 (Cu), 30 (Zn), 0.5 (Ge, Y, W), 2 (Sr, Mo), 0.2 (Nb, Sb), 0.1 (In, Cs, Yb, Hf, Bi), 3 (Ba), 0.05 (La, Ce, Nd, Tl, Th), 0.01 (Pr, Sm, Gd, Tb, Dy, Ho, Er, Ta, U), 0.005 (Eu, Tm), and 0.002 (Lu).

Sr–Nd isotopic analyses

Sr–Nd isotope analyses were conducted at the Center of Instrumental Analysis, Okayama University, Japan. Approximately 70 mg of whole-rock powdered samples were dissolved in a mixture of purified HNO_3–HF–$HClO_4$ in Teflon vials on a hot plate (100–140°C). Separation of Sr and Nd was carried out using a standard two-column ion-exchange technique. Isotopic analyses were carried out at the Center of Instrumental Analysis using a five-collector Finnigan MAT-262 mass spectrometer. Sr and Nd were loaded in 2% H_3PO_4 (repeatedly purified using a cation exchange column) on double Ta–Re filaments and analysed in the static mode. For mass fractionation corrections, the $^{87}Sr/^{86}Sr$ and $^{143}Nd/^{144}Nd$ isotopic data were normalized against the values of $^{86}Sr/^{88}Sr = 0.1194$ and $^{146}Nd/^{144}Nd = 0.7219$, respectively. During the period of data acquisition, the mean of the measured $^{87}Sr/^{86}Sr$ ratios of NBS 987 standard gave 0.710295 ± 11 (2σm; $n = 13$ analyses). The mean of the measured $^{143}Nd/^{144}Nd$ ratios of JNdi-1 standard gave 0.5121428 ± 9 (2σm; $n = 5$ analyses), which corresponds to a La Jolla Nd standard value of 0.511885.